

# Modelling strategies for porous structures as solar receivers in central receiver systems: A review

Avila-Marin, A.L.<sup>1\*</sup>, Fernandez-Reche, J.<sup>2</sup>, Martinez-Tarifa, A.<sup>3</sup>

<sup>1</sup> CIEMAT – Plataforma Solar de Almeria (PSA), Avda. Complutense 40, Madrid E-28040, Spain

<sup>2</sup> CIEMAT – Plataforma Solar de Almeria (PSA), P.O. Box 22, Tabernas-Almeria E-04200, Spain

<sup>3</sup> CIEMAT, Avda. Complutense 40, Madrid E-28040, Spain

\* Corresponding author. Tel.: +34 91 346 6629; E-mail address: [antonio.avila@ciemat.com](mailto:antonio.avila@ciemat.com) (Avila-Marin, A.L.)

## Abstract

An international effort is being made to contribute to greener electricity production. Concentrated Solar Power (CSP) has emerged as the favourite candidate due to the advantages associated with it such as dispatchability, maturity and scalability. Particular interest is raised by Central Receiver Systems (CRSs) due to their ability to work at higher temperatures and concentration factors than Parabolic Troughs. Among the different CRS technologies, Volumetric Absorbers (VAs) working with air have received renewed research interest. VAs consist of porous structures where air is heated directly by the porous matrix. An optimised morphological configuration is essential to increasing the thermal efficiency and minimizing thermal losses. The literature presents a large number of works dealing with VA issues and potentialities, and most of them focus on numerical simulation in order to assess an optimal geometrical design or to point out the best directions in terms of thermal behaviour.

This work presents a comprehensive literature review of the main simulation strategies adopted to evaluate VA performance for use in solar towers. The main methodologies, detail simulation and the homogeneous equivalent method, are presented and discussed. Furthermore, different model strategies such as Computational Fluid Dynamics (CFD) and one-dimensional (1D) models are described in detail, together with the importance of the equilibrium state between the fluid phase and the porous phase (local thermal equilibrium and non-equilibrium). Then, the main methods to determine the radiative heat transfer inside the porous phase are described. The study concludes with a discussion of the main trends in the field, where the homogeneous equivalent method, together with the CFD model and local thermal non-equilibrium, make up the most widely used strategies, in addition to silicon carbide material and foam geometry.

## Highlights

Detail simulation is the most accurate method but with very high computational costs

Homogeneous equivalent method is the most widely used simulation strategy

The main trends include local thermal non-equilibrium with silicon carbide foams

Radiative heat transfer prediction is essential to get realistic absorber evaluation

Complex detail simulation is responsible to check volumetric absorber feasibility

## Keywords

Central Receiver System; Volumetric Absorbers; Detail Simulation; Homogeneous Equivalent Method; Review; Numerical simulation;

## Nomenclature

$d$	Cell diameter	(m)
$d_p$	Particle diameter	(m)
$E$	Emitted energy	(W/m <sup>2</sup> )
$F$	Body forces	(m/s <sup>2</sup> )
$G$	Irradiance	(W/m <sup>2</sup> )
$g$	Gravitational acceleration	(m/s <sup>2</sup> )
$H$	Irradiation energy	(W/m <sup>2</sup> )
$h_v$	Volumetric heat transfer coefficient	(W/(m <sup>3</sup> · K))
$J$	Total radiative energy emitted	(W/m <sup>2</sup> )
$i$	Intensity	(W/m <sup>2</sup> )
$i^+$	Forward intensity	(W/m <sup>2</sup> )
$i^-$	Backward intensity	(W/m <sup>2</sup> )
$i_b$	Black body intensity	(W/m <sup>2</sup> )
$i_\lambda$	Spectral intensity	(W/m <sup>2</sup> )
$I_0$	Incident radiation	(W/m <sup>2</sup> )
$I_{0v}$	Volumetric incident radiation at the inlet	(W/m <sup>3</sup> )
$I_v$	Volumetric incident radiation	(W/m <sup>3</sup> )
$K_1$	Inertial permeability coefficient	(m <sup>2</sup> )
$K_2$	Viscous permeability coefficient	(m)
$k$	Thermal conductivity	(W/(m · K))
$P$	Pressure	(Pa)
$q_r$	Radiative flux	(W/m <sup>2</sup> )
$q$	Heat flux	(W/m <sup>3</sup> )
$S_{rad}$	Solar radiation source term	(W/m <sup>3</sup> )
$T$	Temperature	(K)
$t$	Time	(s)
$z$	Fluid direction normal to the absorber frontal surface	(m)

## Greek symbols

$a$	Absorption coefficient	(1/m)
$\beta$	Extinction coefficient	(1/m)
$c$	Heat capacity	(J/(kg · K))
$k$	Thermal conductivity	(W/(m · K))
$\sigma_{SB}$	Stefan Boltzmann constant	(W/(m <sup>2</sup> · K <sup>4</sup> ))
$\sigma$	Scattering coefficient	(1/m)
$\rho$	Density	(kg/m <sup>3</sup> )
$v$	Velocity	(m/s)
$v_D$	Darcy velocity	(m/s)
$\mu$	Viscosity	(Pa · s)
$\bar{\tau}$	Stress tensor	(kg/(m · s <sup>2</sup> ))
$\bar{\tau}$	Viscous stress tensor	(kg/(m · s <sup>2</sup> ))
$\omega$	Rate of internal heat generation	(W/m <sup>3</sup> )
$\omega$	Solid angle	(rad)
$\lambda$	Spectral	(nm)

**Adimensional parameters**

C	Anisotropic phase coefficient of the media
$F_{kj}$	View factor between surface k and surface j
H	Heat transfer coefficient parameter
i	Photon direction
k	Surface element
j	Surface element
kj	Between surface k and j
N	Conduction-radiation parameter
s	Photon direction
$w_k$	Quadrature weight of each ordinate
$w'_k$	Sum of the quadrature weight
$\varepsilon$	Emissivity
$\alpha$	Absorptivity
$\rho$	Reflectivity
$\bar{\delta}$	Tensor
$\zeta$	Ratio of the solid to fluid conductivities
$\emptyset$	Porosity
$\Phi$	Scattering phase function
$\Gamma$	Passive scalar constant
$\Omega$	Scattering albedo
$\mu$	Polar angle cosine of each ordinate
$\vec{\phantom{x}}$	Vector
$\langle \phantom{x} \rangle$	Volumetric average

**Subscripts**

b	Black body
eff	Effective
f	Fluid
in	Inlet
s	Solid
r	Radiative

**Superscripts**

f	Fluid
s	Solid

**Acronyms**

CFD	Computational fluid dynamics
CRS	Central receiver system
DOM	Discrete ordinate method
DS	Detail simulation
HEM	Homogeneous equivalent method
HTC	Heat transfer coefficient
HTF	Heat transfer fluid
LTE	Local thermal equilibrium
LTNE	Local thermal non-equilibrium
MC	Monte Carlo
PM	Porous medium
PSA	Plataforma solar de Almeria
PS	Pore escale
RTE	Radiative transfer equation
sDS	Simplified detail simulation
SiC	Silicon carbide
STE	Solar thermal electricity
VA	Volumetric absorber/absorbers
1D	One dimensional
2D	Two dimensional
3D	Three dimensional

## 1. Introduction

Fossil fuels have a privileged position in the energy mix due to their high power density and easy transportation and storage, but the gradual increase in energy consumption has caused a lot of greenhouse emissions and contributed to global warming and energy crises. Such energy and environmental issues have fostered the development of renewable energies and sustainable technologies. Among a wide variety of renewable energies choices, solar energy is one of the resources that shows the potential to alleviate energy issues. However, the small fraction of solar energy striking the earth's surface necessitates the development of technology to increase the power per unit of surface [1]. Solar Thermal Electricity (STE) with optical concentration technologies are important candidates for becoming a major clean, renewable energy resource.

Although the main STE design implemented worldwide uses parabolic-trough collector technology, higher plant efficiencies and lower electricity production costs still require innovation to allow operation at higher temperatures and higher solar fluxes, something Central Receiver System (CRS) already does [2, 3]. In CRS, incident solar radiation is redirected by two-axis tracking mirrored collectors called heliostats, in order to concentrate sunlight at a focal point on the absorber surface at the top of a tower where the energy is transferred to a Heat Transfer Fluid (HTF) by radiative/convective mechanisms.

Of the various options for (CRS) design, the first generation of commercial plants are based on mature technological developments, using cavity or external tube receivers with saturated or superheated steam and molten salt schemes respectively [4-6]. In today's context, Volumetric Absorber (VA) technology working with air as the HTF is an option attracting renewed interest.

In theory, this technology can increase the HTF temperature, reduce thermal losses, and produce higher efficiencies in both the receiver and the power cycle [7] because of the theoretical volumetric effect. However, the majority of the VAs tested presented poorer performance than predicted [8]. Thus, extensive numerical work is found in the literature which analyses and optimises the performance of the VA with different degrees of detail.

In order to homogenise the available information about the numerical modelling of porous absorbers used as solar receivers, this work presents a comprehensive review of the different simulation strategies. Section 2 discusses the background of the VA; the main simulation techniques are briefly described in section 3; while the two main simulation methods, detail simulation (DS – Section 4) and the homogeneous equivalent method (HEM – Section 5), are exhaustively described, in addition to presenting the main studies and governing equations used in each. Moreover, the radiative heat transfers in porous VAs together with the main methods of calculating them are presented in section 6, while section 7 presents the final conclusions and outlook.

## 2. Volumetric absorber background

Early in the 1980s, the VA appeared as a promising option with a simpler design, higher maximum allowable flux, smaller aperture size and lower thermal losses [9], than tubular receivers, where the VA is responsible for transforming solar energy into heat.

### 2.1. Operating principles

The basic operating principles of a VA are [8]:

- A porous structure, made of metal or ceramic materials, is installed in the receiver where the impinging solar radiation is absorbed volumetrically.
- The incident radiation heats up the solid phase. Simultaneously, the HTF cools down the solid matrix and is heated up by convection. In this process, solar radiation is transformed into thermal energy.

Fig. 1 compares the solar absorption in tube receivers and porous absorbers. In a tubular receiver the tube's frontal surface is hotter than the HTF, while in a VA, the frontal temperature of the solid matrix is lower than at the exit, and thus the thermal losses are lower in a VA.

Theoretically, the volumetric effect causes the temperature on the irradiated side of the absorber to be lower than the outlet temperature, producing lower thermal losses than tubular receivers because the frontal surface remains at a lower temperature than the outlet fluid. This theoretical concept was first introduced by Fricker in 1983 [9].

Fricker performed some simple supporting calculations that demonstrated the volumetric effect for a wire mesh absorber under homogeneous incident radiation, but despite numerous efforts, its benefits have not been validated by experimentation [8, 10]. The three experimental works in the literature that have come closest to producing the volumetric effect are: the classic work of Menigault et al. [11] with a two slab selective absorber, where the first layer was made of glass-beads transparent to solar radiation but absorbent in the infrared range, and the second layer was absorbent in both spectra, and the recent works of Romero and co-workers [12, 13] demonstrating the volumetric effect over a novel hierarchically-layered fractal-like volumetric absorber, but where the thermal efficiencies were comparable to the state of the art, because the novel absorbers did not achieve high convective heat rates.

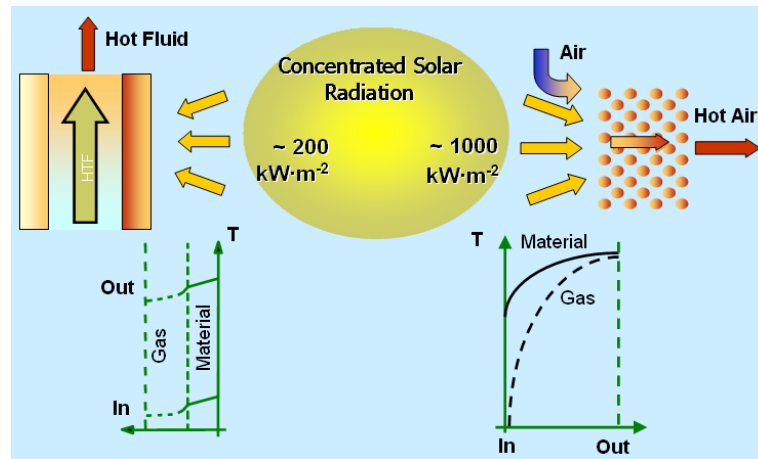


Fig. 1. Performance scheme across a tubular (left) and a volumetric absorber (right) [14]

## 2.2. Conventional absorbers

Usually ceramic materials [15-17] are preferable since the air is able to reach the higher temperatures related to high thermodynamic efficiencies. As a result, metallic materials have not received as much interest, despite the fact that working at lower temperatures offers important thermal advantages [18-20].

The preferred morphological configurations for ceramics are honeycombs and foams made of silicon carbide (SiC). However, despite the large number of scientific studies on the topic, it is not clear yet if ceramics are the best choice in terms of absorber efficiency. Recently, Livshits et al. [21] proposed a VA made of metallic wire mesh as candidate to reach efficiencies higher than 90%.

Avila-Marin [8] presented an exhaustively review of VAs, among which two VAs were considered the baselines for ceramic and metallic absorbers [22]. Concerning the metallic materials, the TSA absorber was tested at the Plataforma Solar de Almeria (PSA). It was made of alloy 601 coiled knit-wire packs. The technical reports highlighted the ability of the VA to achieve 85% thermal efficiency at an air outlet temperature of 700°C, a concentrated solar flux of 300 kW/m<sup>2</sup>, and a recirculation ratio of 60%. The main results of the tests were [23-25]: 1) the operation and control was able to keep the air outlet temperature constant under different working conditions; 2) the modular design could facilitate a scale-up; and 3) the VA was able to match air flow distribution with respect to the incident solar flux. As regards ceramic materials, the SOLAIR absorber was tested at the PSA. The absorber was built of recrystallized SiC with a porosity of 49.5%. The main results showed that the thermal efficiency varied from 70-75% for an air outlet temperature of 750°C with an incident solar flux in the 370-520 kW/m<sup>2</sup> range, and an air return ratio of 50 % [26]. The project success resulted in the construction of a CRS plant with the SOLAIR VA concept in Jülich, Germany that was coupled to a regenerative system and a turbine [27-30].

### 2.3. Operation modes

CRS with VA technology offers three options for commercial implementation:

- Atmospheric system: this choice is the simplest one. It consists of heating the air as it flows through the absorber, and then the hot air is used to heat a second working fluid in a steam generator. Once the steam is produced it is expanded in a Rankine cycle. This system offers the possibility of recirculating the exhausted air to make use of its remaining enthalpy.
- Pressurized system: this option presents a greater challenge than the previous one; however, it offers important benefits as it is used with gas turbines. The most promising design uses solar energy to preheat the air before it enters the gas turbine's combustion chamber, despite it could be used with solar energy in a solo-solar scheme [31].
- Atmospheric-Pressurized system: in the CAPTure project [32], a prototype is being developed where atmospheric air is used to drive a hot air turbine. In that prototype, the high temperature and heat flux part (atmospheric solar receiver) are decoupled from the high pressure part (compressed air stream of the Brayton cycle) via an air-air regenerative heat exchanger (Fig. 2). The regenerative heat exchanger works in alternating modes: non-pressurized heating period, and pressurized cooling period.

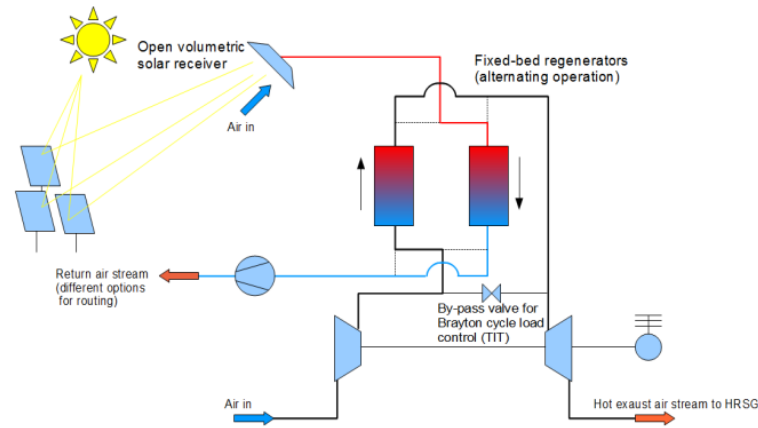


Fig. 2. CAPTure air-air regenerative heat exchanger concept [32-34]



## 2.4. Technology opportunities and concerns

VAs offer important operational opportunities:

- The volumetric absorption of solar radiation [35] allows higher incident flux profiles. Thus, in terms of engineering analysis, the required surface is smaller than that needed in tube receivers.
- The morphological configuration of VAs generally has a large specific surface area and porosity, providing greater contact between the solid and the fluid phases [36].
- CRS using VAs can be brought on line very quickly due to the absorbers' low thermal inertia [37], which reduces the start-up period, and re-start time after transients.
- The HTF is free, reducing plant capital cost, chemically stable at very high temperatures, and does not freeze [38].
- The technology offers thermal energy storage with sensible heat storage tanks [39], and with low-cost materials [40, 41].

Nonetheless, air technology has not had the opportunity to demonstrate its feasibility at the commercial level since some significant challenges need to be addressed. The major concerns are:

- The envisaged volumetric effect has not been fully demonstrated experimentally [10], and if demonstrated, its theoretical benefits have not been observed [13]. To some extent, the feasibility of air technology depends on this effect, without which the receiver's thermal efficiency is poor [8].
- The low HTF thermo-physical properties create the need for very high mass flow rates and very large pipes. This means that a blower with very high power demand is required, thus creating parasitic losses [42].
- VA designs with a linear relation between pressure drop and velocity are candidates for flow instabilities that impede good performance [43, 44].

These issues have received attention in several disciplines, and some of them are inherent in the technology. Nevertheless, a great deal of work is required in order to solve other practical problems, and many of the open questions could be resolved with appropriate numerical strategies that can accurately approximate reality. The intent of this study is to summarise and homogenise the main modelling strategies for VAs, as well as reviewing the most recent and important studies in the literature.

### 3. Simulation techniques

The complex behaviour of VAs complicates its simulation, which can vary in level of detail and usually requires modelling assumptions to simplify the problem. Moreover, when a VA is simulated numerically, it is done in two main phases, the fluid phase and the solid/porous phase. In principle, the simulation methods can be classified into two categories (Fig. 3):

- 1) The Detail Simulation method (DS) is also known as Pore Scale (PS) method. The main difficulties of this simulation are the reconstruction of the real geometry, the generation of the mesh needed to solve equations, and the resources required to solve the governing equations. This approach offers an accurate method at the expense of very high computational costs.
- 2) The Homogeneous Equivalent Method (HEM) is also known as the Porous Medium (PM) method or the volume-average method. This method considers the volume of the receiver with homogenised properties which have been either experimentally determined or have been derived from a numerical DS. The homogenised properties consist of adding semi-empirical terms to the governing equations to consider the effects of the porous media on the fluid flow and heat transfer processes. The main difficulty of this method is the selection of appropriate semi-empirical terms, as its proper selection is crucial to obtaining a successful and accurate model.

After the simulation method is selected, one can differentiate between two types of models (Fig. 3):

- 1) One-Dimensional models (1D): The 1D approach only takes into consideration the changes in the axial direction normal to the frontal surface. Its main advantages are its low computational resource requirements, and the low numerical demand.
- 2) Computational Fluid Dynamics models (CFD): The CFD approach requires specific software to solve governing equations that analyse the changes in axial direction together with other dimensions (2D/3D).

The DS method is linked to the CFD model as it is a 3D simulation that should be performed with software specifically designed to solve microscopic equations. In contrast, the HEM method can use either a 1D or CFD model. The CFD model is adopted when several effects are to be analysed, such as the influence of a Gaussian distribution, a windowed receiver or coupled effects, while the 1D model is usually implemented when optimisation simulations are required.

Once the simulation method (DS or HEM) and the simulation model (1D or CFD) have been selected, the equilibrium state between the two phases of the VA has to be adopted (Fig. 3). Depending on the equilibrium selected, only one phase (fluid) or two phases (fluid and solid) are simulated. There are two equilibrium states available [45]:

- 1) Local Thermal Equilibrium (LTE), which means that the fluid and the solid temperatures are the same [46], neglecting the effect of the heat transfer coefficient (HTC) and the large temperature gradient on the frontal surface of a VA.
- 2) Local Thermal Non-Equilibrium (LTNE), which provides information on the fluid phase and the porous matrix [47]. The energy equations of the fluid phase and the porous phase are coupled by the convective HTC.

The equilibrium selected is quite important; while the LTE approach only solves one energy equation for both phases (as temperature is considered the same for both phases), the LTNE approach solves at least two coupled energy equations, one per phase. Moreover, for the high temperature applications required in solar receivers, the radiative heat transfer has to be calculated, and coupled to the solid energy equation. Thus, the LTNE approach gives more accurate results at the cost of only slightly higher computational costs, which has made it the most widely used approach.

With regard to the LTE approach, it produces the volumetric effect by definition which is not only unrealistic, but wholly incorrect [10]. For example, for an absorber operating under incident fluxes of 800 kW/m<sup>2</sup> with exit air temperature of 1000 °C the predicted efficiency for an ideal LTE absorber is over 95%. Clearly such a simplified model is too optimistic, and more detailed analysis is needed [48].

In summary, both methods, DS and HEM, are acceptable and widely used in the literature. The main differences between them lie in the type of differential equations which need to be solved, and the computational resources needed. While the DS solves microscopic equations in the real geometry and has

very high computational resource requirements, HEM solves macroscopic equations with semi-empirical terms in a volume-averaged geometry needing relatively few computational resources.

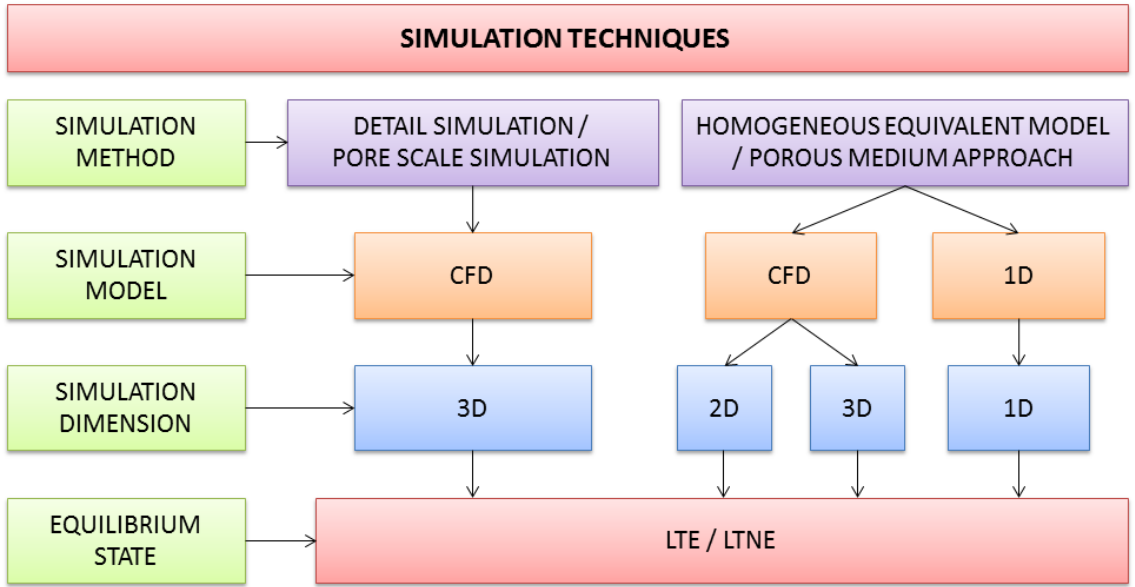


Fig. 3. Simulation techniques that apply to the analysis of volumetric absorber performance

## 4. Detail simulation

DS is the most accurate approach for analyzing the behaviour of a VA. The application of DS has to be performed with CFD software, as 3D geometry is required. Moreover, it has prohibitive computational costs, and there are just few works in the literature following this approach. For that reason, all the available studies only consider a representative volume section to simplify the computational domain. The DS approach is mainly used for two different applications. The following sub-section present the main studies on each type.

### 4.1. Simplified detail simulation

In the following section, a detailed literature review will be presented on the topic of DS in applications other than the complete simulation of a VA, nicknamed simplified detail simulation (sDS). An example of this is the numerical determination of the homogenised properties to be implemented as semi-empirical terms in HEM (Section 5): a) inertial and viscous permeability coefficients, b) effective heat conductivity, c) the convective heat transfer coefficient. This type of simulation is accurate enough to determine individual properties, and less time consuming than the overall simulation of a VA. Table 1 presents a summary of the main sDS studies presented.

Zhao et al. [49] have developed an analytical model for metal foams with idealized cellular morphologies to characterise the radiative transport in terms of radiative parameters: emissivity, reflectivity, and view factors. Radiation was included in the conduction term by means of an effective radiative conductivity (Section 6.3.1). What was proposed was a relatively simple analysis of the radiation heat transfer analysing the net radiation exchange using view factors for the DS known as the Direct Exchange Area Method (Section 6.2).

Petrash et al. [50, 51] have used computer tomography methodology to get a real 3D representation of unstructured foam (Fig. 4a). This technique is useful for inferring structural properties: porosity and specific surface area. Then, a 3D DS was used to get the pressure drop coefficients for the fluid flow equations, and to determine a correlation of the HTC for a Reynolds range between 0.2-to-200. Finally, both data were successfully compared with data in the literature and empirical correlations.

Wu et al. [52] have analysed the fluid flow characteristics through a ceramic foam. The adopted geometry was an idealized periodical structure formed by tetrakaidecahedrons cells (Fig. 4b). The objective was to determine correlations of the pressure drop as function of the main geometrical properties of the foam. The derived correlation was valid for porosity ranging from 66%-to-93%, and for a Reynolds number in the range of 10-to-400. The correlation was compared with existing models and was more accurate for ceramic foams than previous models.

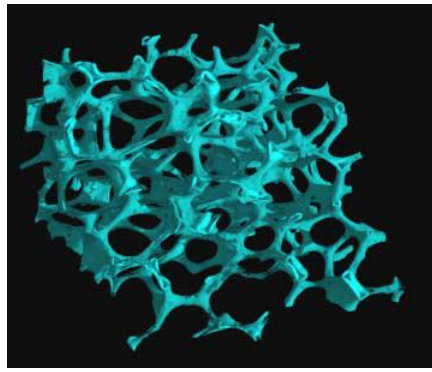
Wu et al. [53] have studied the heat transfer coefficient between a ceramic foam (Fig. 4b) and air in a DS. The sensitivity study focused on several foam parameters such as porosity, velocity, mean cell size and strut temperature. After the simulations, a correlation for the HTC as a function of the Reynolds number and porosity was obtained. The numerical results were checked with available data in the literature, showing good agreement.

Zafari et al. [54] have performed a 3D DS of the heat transfer in metal foams with different porosities (between 85-to-95%). The real geometry was reconstructed with micro-tomography. During the simulations, the solid temperature was set at 800 K, and different velocities were studied. The influence of several parameters over the effective conductivity, pressure drop coefficients, and HTC were analysed. The main conclusions were: 1) a large thermal gradient in the inlet region causes airflow acceleration up to 1.7 times the inlet velocity; 2) the LTE is reached in a relatively short distance; 3) the pressure drop coefficients, the effective conductivity and the HTC are heavily dependent on the porosity and geometrical characteristics.

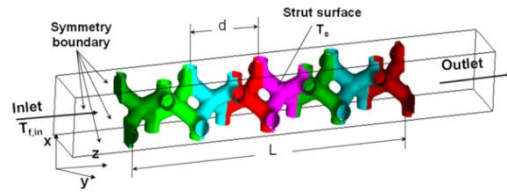
Zhao et al. [55] have constructed a Monte Carlo (MC) method to analyse the optical properties of a SiC foam. A script written in Matlab was used to get the 3D geometry. It gave a correlation between the extinction coefficient and porosity (75-to-95%) and pore diameter (0.4-to-0.6mm). Based on this correlation, the radiative thermal conductivity and radiative heat transfer can be easily computed. Moreover, the numerical results were compared to data in the literature, where good agreement was observed.

Avila-Marin et al. [56] have numerically studied the convective HTC for plain weave wire mesh screens with inline and stagger (Fig. 4c) arrangement. The work focused on a mesh with 1 mm diameter and  $0.2 \text{ mm}^{-1}$  mesh count, and correlations were derived for each arrangement type. The curve fitting was carried out in a HEM, and the results were compared with experimental data, showing good agreement.

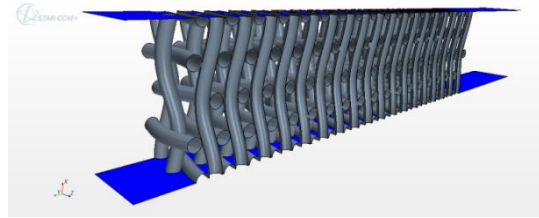
Avila-Marin et al. [57] have dealt with the lack of information in the literature about the HTC with dense wire mesh arrangements. With the goal of finding new correlations for the HTC for stagger arrangement, 3D DS were performed, and the correlations produced were validated. The study focused on the analysis of six types of meshes with stagger arrangement (Fig. 4c), porosities ranging from 47% to 70%, and wire diameter between 1 mm to 0.13 mm. The main conclusions presented were: 1) meshes with different porosities but similar specific surface area have comparable HTC; 2) meshes with similar porosities but different specific surface area perform significantly differently; 3) convective heat transfer increases with the specific surface area.



(a)



(b)



(c)

Fig. 4. Detailed geometries presented in the literature: (a) Petrasch et al. [51]; (b) Wu et al. [52, 53]; (c) Avila-Marin et al.[57]

Table 1. Main characteristics of simplified detail simulation approach

Reference	Year	Method	Model / Dimension	Heat Source	Radiation	Structure	Material	Summary
Zhao et al. [49]	2008	sDS	CFD / 1D	Constant hot and cold temperatures	Conductivity term	Foam	FeCrAlY	Determination of the radiative conductivity
Petrasch et al. [50]	2008	sDS	CFD / 3D	Constant solid temperature	Neglected	Foam	SiC	Computer tomography together with the pressure drop data and HTC correlations
Wu et al. [52]	2010	sDS	CFD / 3D	n.a.	Neglected	Foam	SiC	Generalized parameters to calculate the pressure drop in idealized foams
Wu et al.	2011	sDS	CFD / 3D	Constant solid temperature	Neglected	Foam	SiC	Correlation for the HTC as function of the $\phi$ and Re for idealized foams
Zafari et al. [54]	2015	sDS	CFD / 3D	Constant solid temperature	Neglected	Foam	Aluminum	Analysis of geometrical properties and Nusselt correlation
Zhao et al. [55]	2016	sDS	CFD / 3D	n.a.	Neglected	Foam	SiC	Correlations for the $\beta$ based on the $\phi$ and $d_p$
Avila-Marin et al. [56]	2017	sDS	CFD / 3D	Constant solid temperature	Neglected	Wire mesh	310 alloy	Analysis of the HTC correlation for inline vs. staggered stack wire screens
Avila-Marin et al. [57]	2018	sDS	CFD / 3D	Constant solid temperature	Neglected	Wire mesh	310 alloy	Numerical HTC correlations for staggered stack wire screens

## 4.2. Overall detail simulation

The porous absorbers used with the air technology are responsible for transforming the incident solar radiation into heat, and, due to its morphological design, analysing the fluid flow and heat transfer in the intricate structure is really complex. The comprehensive detail simulation, nicknamed DS, is the most accurate methodology to predict absorber performance. Furthermore, the real fluid flow phenomena and frontal thermal losses can be obtained. This section presents the works available in the literature while Table 2 summarised them.

Michailidis et al. [58] have evaluated the behaviour of nickel foams. The material had a porosity of 92%, and a mean pore size of 0.6 mm. In order to analyse the temperature distribution, CFD simulations were performed over a real geometry obtained by tomography (Fig. 5a). The simulations were performed considering constant heat flux for the walls, and neglecting the thermal radiation. The DS was verified with experimental measurements, and the LTE was checked.

Fend et al. [59] have used two methodologies to predict the fluid flow and heat transfer inside a 3D honeycomb absorber. First, the DS calculated the flow and heat transfer inside a single channel (Fig. 5b) of the original structure. Moreover, the radiative heat transfer was computed with Beer's law (Section 6.1). Secondly, the HEM approach with homogenised properties was computed. It was concluded that both models can be used to predict solid and fluid temperatures profiles, and velocity distributions.

Capuano et al. [60] have presented a 3D CFD simulation for an innovative pin-shaped absorber (Fig. 5c). The simulation took into account heat transfer between fluid and porous phases, and the fluid flow circulating through the structure. The radiation inside the absorber was solved by means of view factors (Section 6.2). The numerical results were compared against experimental data, with a deviation of 3%, and against the ceramic baseline absorber (Section 2), with an improvement in the thermal efficiency of 12%.

Cagnoli et al. [61] have implemented a DS to perform a parametric study of a honeycomb absorber, based on half of a single-channel (Fig. 5d). First, an optical analysis was done with an MC technique to determine the heat flux on the channel's inner walls, which was then used as an input for the 3D DS. The radiative heat transfer was solved with a surface-to-surface model (Section 6.2). The analysis considered three parameters: receiver tilt-angle, channel aperture, and air inlet velocity. The conclusions pointed out that: 1) the value of the tilt angle does not affect channel performance; 2) receiver efficiency increases with the channel aperture; and 3) the combined receiver and power cycle efficiency presents a non-monotonic trend with the inlet velocity.

Recently, Du et al. [62] have published the most comprehensive DS of the performance of a VA. Phenomena including the heat conduction of the porous matrix, the heat convection between the solid and the fluid, and the radiative heat transfer were considered simultaneously. Moreover, the incident solar radiation on the absorber was taken into account by using MC. A tomography technique was used to generate the geometry (Fig. 5e). The geometry involved had 83.5% porosity, 1.02 mm pore diameter and  $1.35 \text{ mm}^{-1}$  specific surface area. The solar radiation was set to  $600 \text{ kW/m}^2$ , and the main conclusions stated were: 1) a DS was successfully built; 2) the fluid temperature inside the porous media exhibits non-uniformity; 3) high conductivity ensures a uniform temperature distribution inside the porous skeleton; 4) HTC varies within a small range along the flow direction; 5) thermal radiation loss is evident in the front surface, and radiative heat transfer becomes dominant with the increase of the average temperature.

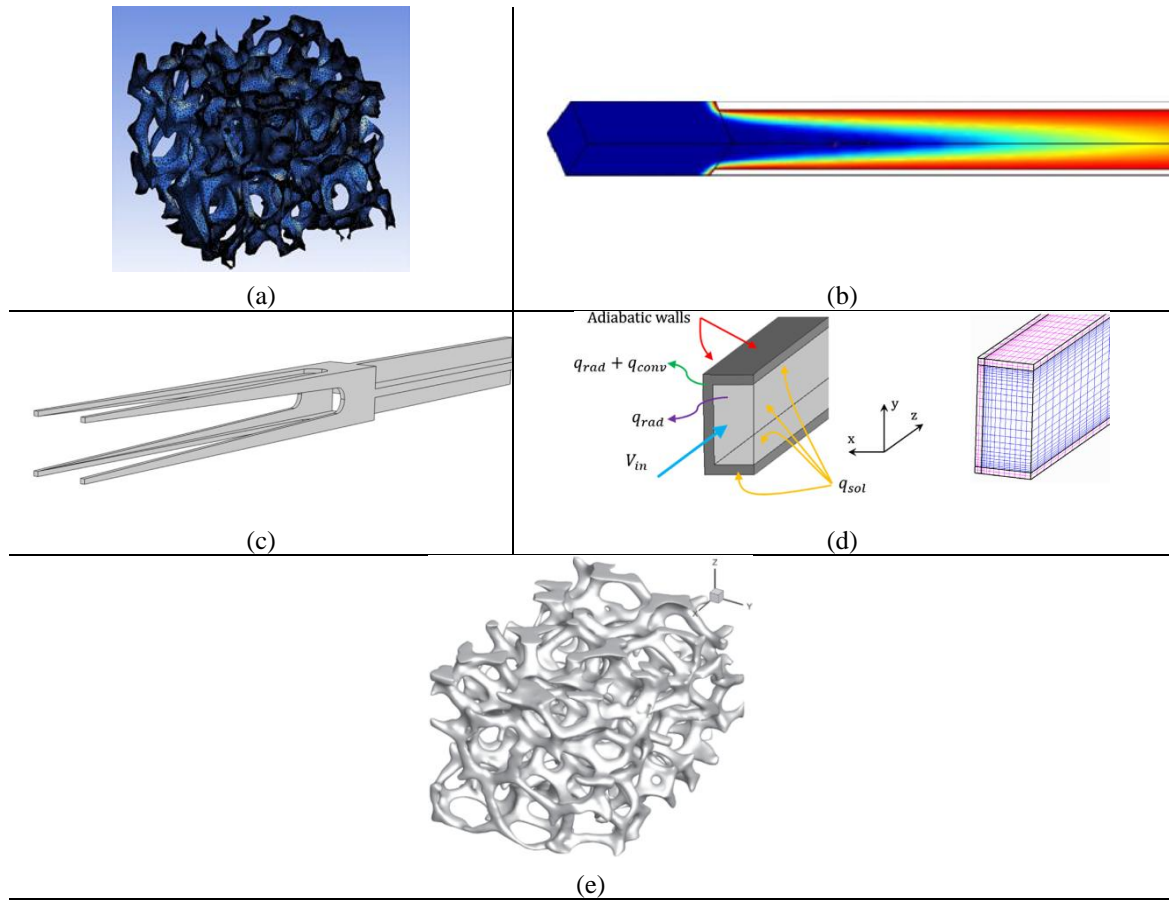


Fig. 5. Detailed geometries presented in the literature: (a) Michailidis et al. [58]; (b) Fend et al. [59]; (c) Capuano et al. [60]; (d) Cagnoli et al. [61]; (e) Du et al. [62];



Table 2. Main characteristics of detail simulation approach

Reference	Year	Method	Model / Dimension	Heat Source	Radiation	Structure	Material	Summary
Michailidis et al. [58]	2013	DS	CFD / 3D	Constant heat flux	Neglected	Foam	Ni	Microstructural analysis, 3D DS and experimental comparison
Fend et al. [59]	2013	DS	CFD / 3D	Solar flux	Exponential attenuation	Honeycomb	SiC	Detail and HEM comparison with experiments. Divergence < 2%
Capuano et al. [60]	2017	DS	CFD / 3D	Solar flux	Surface to surface	Pin-shaped	Titanium-aluminium alloy	New micro-geometry with an efficiency improvement of 12%
Cagnoli et al. [61]	2017	DS	CFD / 3D	Solar flux	Surface to Surface	Honeycomb	Siliconized SiC	Influence of 3 parameters on the design of honeycomb VA
Du et al. [62]	2017	DS	CFD / 3D	Solar flux	MC coupled to CFD	Foam	SiC	Comprehensive 3D CFD simulation of foams coupled to the MC technique

### 4.3. Governing equations

The followings sub-sections present the governing equations, in transient state, to be solved for a porous material used as a solar receiver in the DS approach.

#### 4.3.1. Fluid flow governing equations

Flow modelling in porous media is strongly affected by the internal morphology of the absorber, so its study is very difficult. However, a few works used this approach, and the basic equations used are those of Navier-Stokes [63].

Mass conservation equation:

$$\frac{\partial \rho_f}{\partial t} + \nabla(\rho_f \vec{v}_f) = 0 \quad (1)$$

Momentum equation:

$$\frac{\partial(\rho_f \vec{v}_f)}{\partial t} + \nabla(\rho_f \vec{v}_f \vec{v}_f) = \nabla \bar{t}_f + \rho_f \vec{F} \quad (2)$$

$$\vec{F} = \vec{g} \quad (3)$$

$$\bar{t}_f = -P_f \bar{\delta} + \bar{\tau}_f$$

#### 4.3.2. Energy governing equations

By definition, the DS only uses the LTNE approach. The major simplification is setting the solid temperature as a constant for sDS.

##### 4.3.2.1. Local thermal non-equilibrium

The LTNE approach solves the temperature profiles for both phases, solid and fluid. The basic equations are [64]:

Fluid phase:

$$\frac{\partial(\rho_f c_f T_f)}{\partial t} + \nabla(\rho_f c_f \vec{v}_f T_f) = -\nabla \vec{q}_f + \omega_f \quad (4)$$

Introducing the Fourier law of conduction and considering convective heat exchange between the solid and fluid phase:

$$\vec{q}_f = -k_f \nabla T_f \quad (5)$$

$$\omega_f = h_v (T_s - T_f)$$

Solid phase:

$$\frac{\partial(\rho_s c_s T_s)}{\partial t} = -\nabla \vec{q}_s + \omega_s \quad (6)$$

Similar to the fluid phase, introducing the Fourier law of conduction and considering convective heat exchange between the solid and fluid phase and radiative heat transfer:

$$\begin{aligned} \vec{q}_s &= -k_s \nabla T_s \\ \omega_s &= h_v(T_f - T_s) - \nabla \vec{q}_r \end{aligned} \quad (7)$$

The radiative heat transfer ( $\nabla \vec{q}_r$ ) can be solved with the different methods presented in section 6.

### 4.3.3. Boundary conditions

The boundary conditions are the constraints needed to solve the problem. Their correct selection is crucial to get reliable results as the numerical results can vary significantly between different boundary conditions, and the boundary conditions can vary significantly from one simulation strategy to another. Moreover, it is highly recommended to verify the results with experimental data in order to check the validity. Here, the most usual boundary conditions for DS are presented.

#### 4.3.3.1. Inlet conditions

- 1) Fluid phase: The fluid velocity is set at an inlet velocity, and static temperature, normally 300 K.
- 2) Solid phase: The frontal solid surface is exposed to a combination of incident radiation minus the thermal losses by convection and radiation to the environment:

$$(k_{eff,s} \nabla T_s) = I_0 - h_a (T_s - T_{amb}) - \varepsilon \sigma_{SB} (T_s^4 - T_{amb}^4) \quad (8)$$

- 3) Solar flux profile: The incoming concentrated solar incident flux ( $I_0$ ) is a crucial boundary, and it is usually implemented in different ways. The main choices for DS are the following:
  - a) The simplest approach is to consider the incident solar flux as a constant at the absorber's aperture.
  - b) The most complex approach is to use a Monte Carlo method to calculate the radiation distribution at the frontal surface.

#### 4.3.3.2. Outlet conditions

- 1) Fluid phase: The temperature gradient at the fluid outlet surface and the static pressure (with a reference pressure of 101325 Pa) are set to zero.
- 2) Solid phase: The temperature gradient at the solid outlet surface is set to zero.

## 5. Homogeneous equivalent method

HEM is a faster modelling strategy, however, the accuracy of its results are tightly linked to the homogenised properties adopted. Most engineering applications are normally focused on macroscopic phenomena instead of the analysis at the pore level. Indeed, when the macroscopic model is adopted, there is no need to describe the entire complex geometry of the porous media.

HEM allows both model types (Fig. 3): 1D, and CFD, and the equations to be solved are the same in both models. The VA is modelled as a homogeneous effective medium comprising two continuous phases, solid and fluid. This is the usual strategy where the method averaged the governing equations into elemental volume cells that are larger than the detail scale but smaller than the whole geometry [65].

### 5.1. 1D model

In the following, the most important investigations are highlighted for HEM with 1D model (Fig. 3). Table 3 presents a summary of the main works.

Pitz-Paal et al. [66] have performed an important experimental and numerical study of the thermal performance and flow stability of four different VAs under a non-homogeneous irradiation profile. The LTNE approach together with the Discrete Ordinate Method (DOM – Section 6.3.3) was adopted. Good agreement was found between the numerical and experimental results for all the absorbers considered. As a notable result, flow instability was found only in structures with a linear relation between pressure drop and velocity.

Bai et al. [67] have investigated the fluid flow performance over a foam under uniform heat flux using the LTE approach. It was concluded that fluid flow resistance decreases with decreasing air outlet temperature, mainly due to the decrease in air viscosity. Thus, a non-homogeneous incident radiation at the frontal surface will cause areas with higher flow resistance producing higher air flow in the cold area, keeping the hot areas even less cooled, which is one of the main reasons for the flow instabilities.

Xu et al. [68] have developed a 1D model with the LTNE approach without considering thermal radiation inside a foam. The study was a parametric one of porosity, particle diameter, and thickness. It was argued that the bigger the particle diameter, the higher the solid temperature, and the greater the porosity or the sample thickness, the lower the solid temperature and the higher the fluid temperature, which are important fundamentals for the geometric optimisation of the absorber.

Sano et al. [69] have established analytical expressions for a foam to study its pressure and temperature profiles. The 1D model used the LTNE approach together with the Rosseland conductivity approximation (Section 6.3.1). After the analytical expressions were validated, the heat transfer and fluid flow were analysed to avoid flow instabilities and hot spots. The work concluded that the pore diameter must be larger than a critical value to ensure high VA efficiencies. The optimum pore diameter could be derived from an analytical equation.

Mey et al. [70] have built a 1D model with the LTNE approach focusing in the study of three different radiative models and the comparison against the results obtained with an MC algorithm for a foam. After comparing the results, it was concluded that the two-flux approximation are an appropriate approximation to solve the radiation inside a porous absorber.

Kribus et al. [10] have analysed the performance of a VA based on its geometrical and material properties. A 1D model with the LTNE approach was used for foam. The work emphasized the radiative heat transfer, and 4 different models were implemented. After the analysis, the discrete ordinate method  $S_4$  (section 6.3.3.2) was selected for parametric studies due to its accuracy and fast computation. The work confirmed the strong influence of porosity on thermal efficiency. Moreover, the optimisation of foam geometry did not result in higher efficiencies. Based on the results, there are two choices for improving the thermal efficiency: 1) a significant increase in the HTC, and 2) the implementation of newer materials with spectral selectivity.

Wang et al. [71] have studied a foam with the LTNE approach, and with the Rosseland approximation (Section 6.3.1). Three parameters were adopted: the conduction-radiation parameter ( $N$ ), the ratio of the solid to fluid conductivities ( $\zeta$ ), and the HTC ( $H$ ). The main conclusions were: 1) increasing  $N$  at a constant  $H$  decreases the solid temperature at the inlet and increases the fluid temperature at the outlet; 2) the transported radiative energy increases with  $N$ , while it decreases with an increase in  $\zeta$ .

Li et al. [72] have investigated the dynamic behaviour of a VA with thermal energy storage. The analysis of the foam was performed with the LTNE approach, and with the Rosseland approximation (section 6.3.1). The results were compared with experimental data, showing good agreement, with deviations in

the absorber model of less than 10%, and less than 7% in the thermal energy storage.

Wang et al. [73] have developed a 1D model with the LTNE approach, and  $P_1$ -approximation (Section 6.3.2) to perform two studies: an analysis of the porosity linear variation and a study of the pore diameter linear variation. Moreover, three cases were considered: Increasing (I), Decreasing (D), and Constant (C). The work showed that porosity distribution type D performed better than type I, due to better penetration of the incident irradiation into the foam. Finally, a D porosity layout combined with I pore scheme was the best configuration for the energy transfer.

Wang et al. [74] have studied a windowed foam experimentally and numerically. The LTNE approach and the  $P_1$ -approximation (Section 6.3.2) were adopted. The windowed cavity was simulated considering two infinite parallel planes. The work found the Karr and Dybbs HTC correlation [75] to be the one that better matched the experimental results. The main conclusions obtained were: 1) window thermal losses decreases when solid thermal conductivity increases; 2) the temperature profile of the VA phases increases when the glass emissivity decreases; 3) the opposite effect was detected for solid phase emissivity; and 4) the maximum deviations between the numerical results and the tests were below 10% and 3% for the back wall temperature and the air outlet temperature, respectively.

Zaversky et al. [76] have presented two models with the LTNE approach and two radiative heat transfer techniques. The first used the Rosseland approximation (section 6.3.2), while the second used the discrete ordinate method (section 6.3.3). Both strategies were successfully compared with experimental tests. Then, a parametric optimisation was carried out over geometrical parameters: porosity, thickness, cell diameter and density. The results show that: 1) absorber thermal efficiency is directly related to its porosity; 2) maximum absorber efficiency is obtained for cell densities between 30-50 PPI; and 3) graded porosity configuration does not improve on the performance of single porosity foams.

Table 3. Main characteristics of 1D homogeneous equivalent method

Reference	Year	Method	Model / Dimension	Heat Source	Radiation	Structure	Material	Summary
Pitz-Paal et al. [66]	1997	HEM	1D / 1D	LTNE	DOM – $S_6$	Corrugated foil Honeycomb Wire mesh Foam	$X_5CrAl_2O_5+Ce$ SiC Alloy 601 SiC (50-60%)	Thermal analysis and flow stability study for four absorbers
Bai et al. [67]	2010	HEM	1D / 1D	LTE	-	Foam	SiC	Study of the air flow resistance
Xu et al. [68]	2011	HEM	1D / 1D	LTNE	Neglected	Foam	SiC	Parametric study of $\phi$ , $d_p$ , $v_{in}$ and absorber thickness
Sano et al. [69]	2012	HEM	1D / 1D	LTNE	Rosseland	Foam	SiC	Analytical solutions for the optimal pore diameter and absorber thickness
Mey et al. [70]	2014	HEM	1D / 1D	LTNE	Rosseland $P_1$ model Two flux MC method	Foam	SiC	Study of different radiative models
Kribus et al. [10]	2014	HEM	1D / 1D	LTNE	$P_1$ model Two flux DOM – $S_4$ MC method	Foam	SiC	Exhaustive analysis of radiative models and analysis of main foams challenges
Wang et al. [71]	2014	HEM	1D / 1D	LTNE	Rosseland	Foam	SiC	Parametric analysis for three dimensionless parameters
Li et al. [72]	2016	HEM	1D / 1D	LTNE	Rosseland	Foam	SiC	Dynamic simulation of volumetric absorber and thermal energy storage
Wang et al. [73]	2017	HEM	1D / 1D	LTNE	$P_1$ model	Foam	-	Study of porosity and pore diameter linear variation
Wang et al. [74]	2017	HEM	1D / 1D	LTNE	$P_1$ model	Foam	SiC	Thermal analysis of a windowed absorber installed in a parabolic dish
Zaversky et al. [76]	2018	HEM	1D / 1D	LTNE	Rosseland DOM – $S_8$	Foam	SSiC	Two-model comparison against experiments. Parametric study of geometric parameters of foams

## 5.2. CFD model

This section presents a literature review of HEM with the CFD model according to the chronological appearance of the studies, and Table 4 summarises the main works.

Wu et al. [77] have developed a macroscopic 2D CFD model for a foam. The model considered the LTNE approach and the  $P_1$ -approximation. The model carried out a sensitivity analysis over: inlet velocity, porosity, mean cell size and solid conductivity. Finally, the results were compared with experimental data. The work concluded that the best absorber thermal efficiency is achieved with a cell size of 1-2 mm together with the highest possible porosity.

Wu et al. [78] have presented a 2D HEM with the LTNE approach to study the transient performance of foams. The  $P_1$ -approximation is established, and the incident flux was derived from a Gaussian distribution. The work concluded that under sudden changes, the VA's reaction time varies between 30-70 seconds and the pressure drop reacts smoothly.

Cheng et al. [79] have analysed a pressurized absorber with a CFD model under the LTE approach. The incident flux distribution behind the quartz window was calculated with a Monte Carlo script, then, the results were coupled to the CFD. The work focused on the analysis of geometric parameters of the concentrator and the properties of the absorber. Among the more remarkable conclusions presented are several curves that allow the optimal thickness of the absorber to be determined.

Wang et al. [80] have studied the performance of foams with CFD software, the LTNE approach, and the Rosseland approximation (section 6.3.1). A Monte Carlo method was set to obtain the heat flux distribution over the surface. The main conclusions were: 1) the heat flux distribution over the surface has a strong influence on the temperature profiles; 2) the maximum solid temperature and the thickness of the LTNE increases with the porosity; 3) the frontal temperature difference between the solid and fluid increases with the mass flow; 4) the temperature of the solid decreases conversely to the emissivity; and 5) the maximum temperature of the solid increases with the particle diameter.

Wang et al. [81] have studied the coupled behaviour of a parabolic dish with a VA. A Monte Carlo method was established to get the heat flux over the absorber surface, while a 2D CFD was adopted with the LTNE approach, and the Rosseland approximation (section 6.3.1). The work was a parametric study with the following variables: solar irradiance, inlet velocity, particle diameter, receiver dimensions, and air properties. The main conclusions drawn were: 1) solid foam temperature increases with both solar irradiance and particle diameter; 2) porous temperature decreases with increasing inlet velocity and receiver radius; and 3) the properties of the air have a negligible effect.

Wang et al. [82] have carried out a study of two different radiative approximations (Rosseland and  $P_1$ -approximations) inside a foam. The VA was modelled using the LTNE approach. It was concluded that the maximum temperature difference between both models is 5%, and the maximum temperature difference is higher for the  $P_1$ -approximation than for the Rosseland approximation.

Fuqiang et al. [83] have analysed the heat flux gradient and the inlet fluid location (Fig. 6a) in a porous absorber with a quartz window. The irradiation passing through the window and striking the absorber was computed with a Monte Carlo method. The absorber was foam, and it was analysed numerically with CFD software adopting the LTNE approach, and the Rosseland approximation (section 6.3.1). The study pointed out that the peak flux over the VA decreases when introducing the quartz window, the fluid inlet location changes the pressure and temperature distribution considerably, and the solid temperature increases with the porosity.

Roldan et al. [84] have evaluated the performance of graded porosity. The simulation of a honeycomb absorber was performed with 2D CFD software and with the LTE approach. The study was divided into: 1) constant porosity, 2) graded (increasing and decreasing) porosity in the radial direction, 3) graded (increasing and decreasing) porosity according to the absorber's depth. The incident heat flux followed a Gaussian distribution, and the contribution of the solar radiation was included in the fluid energy equation (section 5.3.2.2) with Beer's law (section 6.1). The work concluded that decreasing porosity configuration according to the absorber's depth produced a thermal improvement compared to the other configurations.

Chen et al. [85] have investigated the effect of the geometrical properties of double-layer foams (Fig. 6b). A CFD model with the LTNE approach, and the  $P_1$ -approximation was adopted. The work concluded that the thickness of the first layer critically affects the temperature field and pressure drop, and better performance is obtained when the second layer porosity is thinner than the first.

Meng et al. [86] have designed a new VA using cup-shaped alumina foam with a quartz window (Fig. 6c). The irradiation was provided by a parabolic dish, and a Monte Carlo method was adopted to obtain the profile. A CFD model, with the LTNE approach, and the Rosseland approximation was applied to solve the heat transfer. The main conclusions drawn were: 1) the cup-shaped design improves on the performance of flat absorbers, decreasing the porous temperature; and 2) the alumina material achieves lower thermal losses and higher air outlet temperatures than silicon carbide.

Chen et al. [87] have constructed a model with a VA and a parabolic dish (Fig. 6d), and analysed the optical error of the parabolic dish, and used two approaches for the concentrated solar radiation: thermal boundary condition and collimated incident radiation. The solar radiation transport was simulated with a Monte Carlo method, and the VA performance was analysed with CFD software, the LTNE approach, and the  $P_1$ -approximation. The main conclusions were: 1) geometrical parameters affect the solar distribution within the absorber, 2) the thermal boundary condition approach overestimates the frontal porous temperature and underestimates the air outlet temperature, and 3) the collimated incident radiation approach provides an acceptable temperature field.

Roldan et al. [88] have analysed the influence of the wind, and recirculated air for the HiTRec absorber [89]. It was simulated in 2D CFD software under the LTE approach (Fig. 6e). The thermal radiation contribution was added to the fluid energy equation following Beer's law (section 6.1). It was concluded that: 1) outlet air temperatures perform inversely to external wind velocity and the incidence angle; 2) the outlet air temperature increases with the temperature of the recirculated air and decreases with the inlet velocity of the recirculated air.

Chen et al. [90] have done the analysis of composite structures. The composite consisted of a porous absorber where different geometric properties were adopted in a predetermined region at the inlet and near the wall of the absorber (Fig. 6f). CFD software with the LTNE approach and the  $P_1$ -approximation was used. The work compared composite absorbers with conventional ones. The results indicated that a composite configuration, with low porosity and small cell size in the inlet near-wall region, reduces the usual temperature gradient in the porous phase.

Zhu et al. [91] have presented a new foam with a high heat transfer and a low pressure drop. The geometry was formed of packed strut cross-shaped particles (Fig. 6g) with spectral properties. The absorber was simulated with CFD software, the LTNE approach, and the discrete ordinate method (Section 6.3.3). A parametric study was performed over the pore size, porosity, spectral emissivity and Heywood factor (Fig. 6g). The main conclusions were: 1) the spectral selectivity and strut shape can improve efficiency; 2) the extinction coefficient has an important influence on the thermal losses; 3) efficiency increases with the porosity and the Heywood factor.

Du et al. [92] have coupled a genetic algorithm with the heat transfer mechanisms, to optimise the parameters that guarantee the best performance. The VA model was done with CFD software, the LTNE approach, and the Rosseland approximation (Section 6.3.1). Two types of optimisations were studied: 1) a single-objective optimisation concluded that efficiency is enhanced for both large porosity and inlet velocities, and in addition, pore size should increase with the thickness of the VA; 2) a multi-objective optimisation yielded a Pareto front plot as a function of flow resistance and thermal efficiency to select appropriate parameters.

Teng et al. [93] have simulated a new configuration, where the receiver was placed at the top of the tower and parallel to the ground. In front of the absorber, several coated mirrors were joined in a circular-shape reflector (Fig. 6h). The purpose of these mirrors was to reflect part of the radiation losses coming from the absorber. The data were analysed in 2D CFD software with the LTNE approach and the  $P_1$ -approximation (section 6.3.2). The work concluded that 65% of the emitted radiation was reused in the absorber achieving an air outlet temperature of 1352 K and 88.6% efficiency. The same absorber without the mirror systems achieved an air outlet temperature of 1265 K and 81.3% efficiency.

Du et al. [94] have analysed a multi-aiming point strategy and air inlet parameters over the heat transfer and stress characteristics of a pressurized absorber. The same numerical model applied by Cheng [79] was implemented here. The main conclusions were: 1) the solar distribution over the aperture and absorber are more uniform, and the peak flux can be reduced by an order of magnitude compared to the single aiming point strategy; 2) increasing the air inlet temperature from 350-to-550 K results in an increase in the absorber temperature, the window temperature and the window of 20%, 31% and 62% respectively; 3) reducing the mass flow rate can produce local overheating.

Nimvari et al. [95] have simulated a new inlet velocity distribution in order to minimize the temperature gradient in the absorber. A Fortran program was written with the LTNE approach and  $P_1$ -approximation. The incident flux followed a Gaussian distribution. The study successfully examined the ability of the non-uniform air velocity distribution at the inlet boundary to decrease the maximum solid temperature



and its gradient, causing the maximum temperature to move deeper into the solid phase.

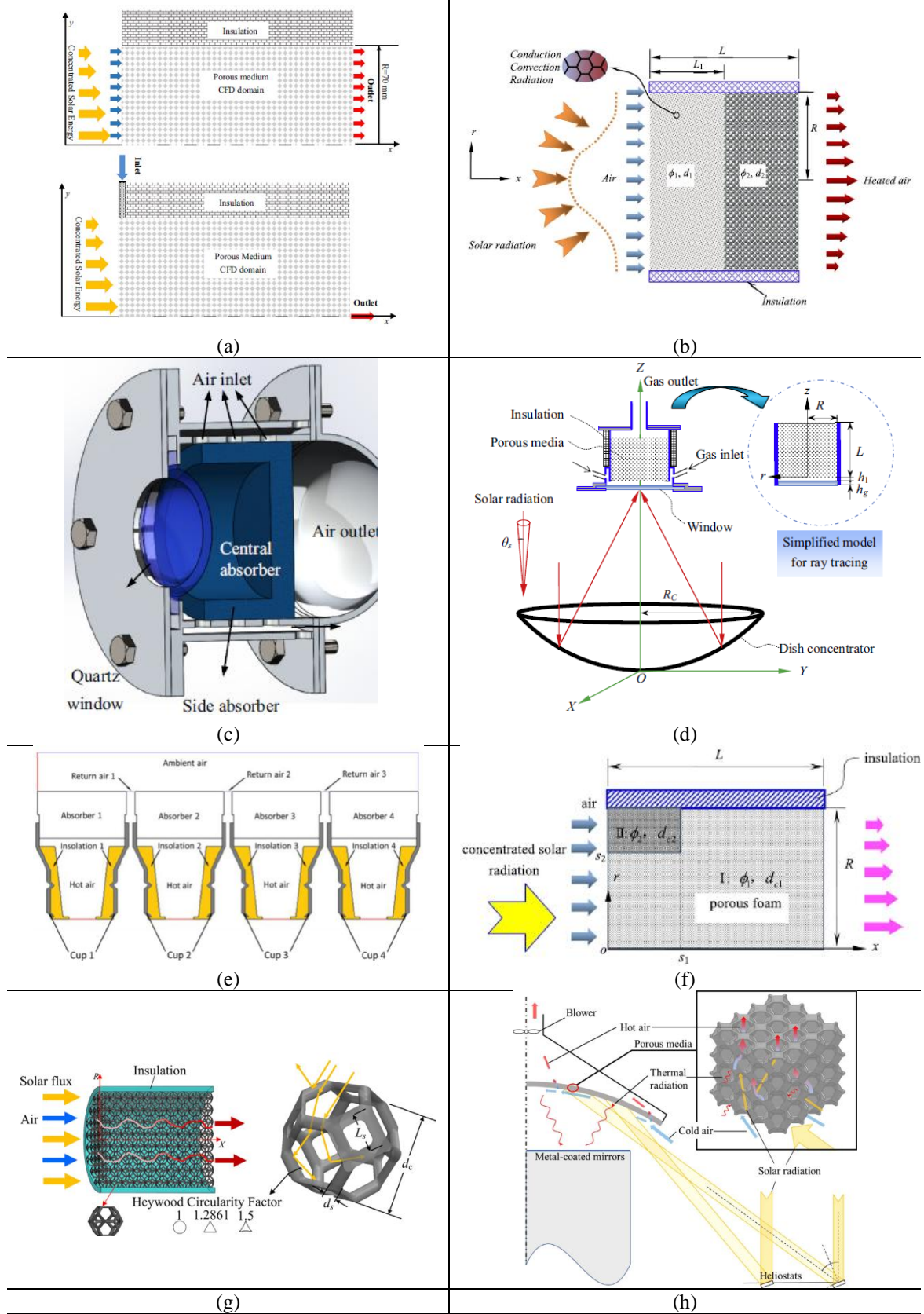


Fig. 6. Geometries used in the CFD software presented in the literature: (a) Fuqiang et al. [83]; (b) Chen et al. [85]; (c) Meng et al. [86]; (d) Chen et al. [87]; (e) Roldan et al. [88]; (f) Chen et al. [90]; (g) Zhu et al. [91]; (h) Teng et al. [93];

Table 4. Main characteristics of CFD homogeneous equivalent method

Reference	Year	Method	Model / Dimension	Heat Source	Radiation	Structure	Material	Summary
Wu et al. [77]	2011	HEM	CFD / 2D	LTNE	P <sub>1</sub> model	Foam	SiC	Parametric study of $v_{in}$ , $\phi$ , $d$ , and $k_s$
Wu et al. [78]	2011	HEM	CFD / 2D	LTNE	P <sub>1</sub> model	Foam	SiC	Transient analysis of the VA under heat flux changes
Cheng et al. [79]	2013	HEM	CFD / 2D	LTE	DOM	Foam	-	Analysis of geometric parameters of the concentrator and the properties of the absorber
Wang et al. [80]	2013	HEM	CFD / 2D	LTNE	Rosseland	Foam	SiC	Influence of heat flux, thermal losses, $\phi$ , $\epsilon$ , $d$ , and $v_{in}$
Wang et al. [81]	2013	HEM	CFD / 2D	LTNE	Rosseland	Foam	SiC	Parametric study over the solid temperature
Wang et al. [82]	2014	HEM	CFD / 2D	LTNE	Rosseland P <sub>1</sub> model	Foam	SiC	Study of the two commonly used approximations for the RTE
Fuqiang et al. [83]	2014	HEM	CFD / 2D	LTNE	Rosseland	Foam	SiC	Present the influence of two possible fluid inlet configurations over a windowed receiver
Roldan et al. [84]	2014	HEM	CFD / 2D	LTE	Beer law	Honeycomb	SiC	Thermal analysis of graded porosity absorbers
Chen et al. [85]	2015	HEM	CFD / 2D	LTNE	P <sub>1</sub> model	Foam	SiC	Thermal analysis of graded porosity ceramic foams
Meng et al. [86]	2016	HEM	CFD / 3D	LTNE	Rosseland	Foam	Al <sub>2</sub> O <sub>3</sub>	Propose a new windowed cup-shaped alumina absorber
Chen et al. [87]	2016	HEM	CFD / 2D	LTNE	P <sub>1</sub> model	Foam	SiC	Evaluate two different approaches for the incident radiation
Roldan et al. [88]	2016	HEM	CFD / 2D	LTE	Beer law	Honeycomb	SiC	Influence of the external wind conditions and recirculated air
Chen et al. [90]	2017	HEM	CFD / 2D	LTNE	P <sub>1</sub> model	Foam	SiC	Solve the behaviour of foams with different geometrical properties in the inlet near-wall region
Zhu et al. [91]	2018	HEM	CFD / 2D	LTNE	DOM	Foam	SiC	Parametric study over a spectral dependent SiC foam
Du et al. [92]	2018	HEM	CFD / 2D	LTNE	Rosseland	Foam	SiC	Couple genetic algorithm with the

								thermal analysis of foams to obtain appropriate parameters
Teng et al. [93]	2018	HEM	CFD / 2D	LTNE	P <sub>1</sub> model	Foam	SiC	Simulation of a receiver together with metal mirrors in order to reduce thermal losses
Du et al. [94]	2018	HEM	CFD / 3D	LTE	DOM	Foam	SiC	Analysis of pressurized volumetric absorber with multi-point aiming strategy
Nimvari et al. [95]	2018	HEM	CFD / 2D	LTNE	P <sub>1</sub> model	Foam	SiC	Analysis of the velocity distribution over the solid temperature of the foam

### 5.3. Governing equations

The followings sub-sections present the governing equations, in transient state, to be solved for a porous absorber with HEM.

#### 5.3.1. Fluid flow governing equations

The fluid mass flow is constant through each cross section for 1D simulation, and through each volume-averaged cell for CFD simulations, by means of the continuity equation. Concerning the momentum equations, the flow through a porous media is modelled with Darcy's law to describe slow or creeping flows, and Forchheimer's law for high velocity flows.

Mass conservation equation:

$$\frac{\partial \rho_f}{\partial t} + \nabla(\rho_f \bar{v}_f) = 0 \quad (9)$$

Momentum equation:

$$\frac{1}{\phi} \frac{\partial(\rho_f v_D)}{\partial t} + \frac{1}{\phi^2} \nabla(\rho_f v_D v_D) = -\nabla \langle P_f \rangle^f + \frac{\mu_f}{\phi} \nabla^2 v_D - \frac{\mu_f}{K_1} v_D - \frac{\rho_f}{K_2} |v_D| v_D \quad (10)$$

#### 5.3.2. Energy governing equations

There are two approaches for modelling the equilibrium state: LTE and LTNE. The LTE approach gives the volumetric effect by definition, as it assumes the convection heat transfer between the solid and fluid at the absorber walls to be infinite, which is unrealistic. As a result, this approach might be ruled out when modelling volumetric absorbers. More realistic estimates can be produced with the LTNE approach as it takes into consideration the HTC between the porous matrix and the fluid.

##### 5.3.2.1. Local thermal non-equilibrium

In this approach, the two phases (solid and fluid) are spatially coincident and only interact with regard to the HTC.

Fluid phase:

$$\nabla(\langle \rho_f c_f T_f \rangle^f v_D) = \nabla(k_{eff,f} \nabla \langle T_f \rangle^f) + h_v (\langle T_s \rangle^f - \langle T_f \rangle^f) \quad (11)$$

Solid phase:

$$0 = \nabla(k_{eff,s} \nabla \langle T_s \rangle^s) + h_v (\langle T_f \rangle^s - \langle T_s \rangle^s) - \langle \nabla q_r \rangle \quad (12)$$

##### 5.3.2.2. Local thermal equilibrium

This approach only solves the fluid energy equation (Eq. (13)), including a source term to compute the contribution of the concentrated solar radiation ( $S_{rad}$ ). That energy source term,  $S_{rad}$ , follows a simplified approach to the solar flux, defining an exponential attenuation, as derived from Beer's law [96] (Section 6.1).

Fluid phase:

$$\nabla(\langle \rho_f c_f T_f \rangle^f v_D) = \nabla(k_{eff} \nabla \langle T_f \rangle^f) + S_{rad} \quad (13)$$

$$S_{rad} = \beta I_0 \exp^{-\beta z} \quad (14)$$

### **5.3.3. Boundary conditions**

The boundary conditions needed for the HEM are similar to those for the DS. The main difference is related to the implementation of the solar flux profile at the inlet which is easier in the HEM and the effective properties needed for the governing equations. It is highly recommended to verify the numerical results with experimental data in order to assure the accuracy of the results as the numerical modelling can vary significantly between different boundary conditions.

#### **5.3.3.1. Inlet conditions**

- 1) Fluid phase: The fluid velocity is set at an inlet velocity, and static temperature, normally 300 K.
- 2) Solid phase: The temperature gradient at the solid outlet surface is set to zero.
- 3) Solar flux profile: The incoming concentrated solar incident flux could be implemented in three different ways:
  - a) Constant incident solar flux profile [77]
  - b) Gaussian flux profile [90]
  - c) Real solar flux profiles [97]

#### **5.3.3.2. Outlet conditions**

- 1) Fluid: The temperature gradient at the fluid outlet surface and the static pressure (with a reference pressure of 101325 Pa) are set to zero.
- 2) Solid: The temperature gradient at the solid outlet surface is set to zero.

## 6. Radiative heat transfer

The radiative heat transfer inside a porous receiver is an essential heat transfer mechanism, and its solution is crucial for a good approximation to reality. There are three ways to compute it:

- 1) Analytical simplified method: The exponential decay of the radiation is produced by multiple reflection-absorption processes. This simplified method can serve as an initial approach because of its lower CPU demand, but its accuracy is somewhat limited.
- 2) Direct exchange area method: This method accounts for the radiation exchange between the surfaces of an enclosure. This approach is used for periodical structures with relatively simple geometries.
- 3) Radiative transfer equation (RTE): The RTE accounts for the absorbing, emitting, and scattering processes of the medium. Several approaches exist for its solution (section 6.3).

### 6.1. Analytical simplified method

Beer's law represents the exponential decay of the incident radiation [98]. It is usually used to get the attenuation by absorption of the impinging radiation, as presented in Eq. (15):

$$I = I_0 \exp^{-\beta z} \quad (15)$$

When it is implemented in the energy equation, a volumetric heat source has to be defined as follows [84]:

$$\nabla q_r = \beta I_0 \exp^{-\beta z} \quad (16)$$

This assumption requires very few computational resources and could be considered an acceptable approach to describe the radiation penetration in the absorber; however, the level of detail about the radiative process is weak, as it does not include radiative interactions due to the multiple light reflection, scattering and absorption [99]. Nevertheless, the accuracy of the whole strategy could be increased if the boundary condition were properly derived.

The boundary condition adopted for this radiative approach is that presented in Eq. (8), and it is accepted for both modelling strategies (DS and HEM).

## 6.2. Direct exchange area method

The direct exchange area method [100] is also known as the surface-to-surface method [101]. This approach arose because, in many applications, the radiation exchange occurs between the walls of an enclosure that are well defined (Fig. 5c-Fig. 5d). The main assumption of this method is that any absorption, emission, or scattering of radiation can be ignored; therefore, only surface-to-surface radiation needs to be considered.

This method can be applied according to four different levels of complexity. The most common and accepted simplification is when the surfaces are assumed to be grey and diffusive [98]. This simplification means that the radiative properties of the surfaces do not depend on wavelength, and emit as well as reflect energy diffusely.

In general enclosures, the irradiation ( $H$ ) on a surface element has contributions from all visible surfaces. Thus, it is necessary to determine the amount of energy leaving a surface toward other visible surfaces. The energy exchange between two surfaces depends in part on their size, separation distance, and orientation. These parameters are accounted for by a geometric function called the view factor. The view factor is a geometrical relation, and represents the fraction of energy leaving one surface which is intercepted by a second surface.

The total radiative energy emitted (radiosity),  $J$ , leaving a surface element is the sum of the emitted and reflected energy:

$$J = E + \rho H \quad (17)$$

For a domain with a grey-diffusive surface, the radiative energy that is given off by a surface element  $k$ , is computed according to the following relation [61, 101]:

$$J_k = \varepsilon_k \sigma_{SB} T_k^4 + \rho_k \sum_{j=1}^N J_j F_{kj} \quad (18)$$

This method is useful for periodical structures with relative simple geometry (Fig. 5c-Fig. 5d), so the direct exchange area method is the preferred option due to its high accuracy with an acceptable computing demand.

The divergence of the total radiative heat transfer necessary to couple it with the solid energy equation is:

$$\nabla q_r = \varepsilon (J_k - \varepsilon \sigma_{SB} T_s^4) \quad (19)$$

Concerning the boundary condition, the same used in Eq. (8) applies for the direct exchange area method.

### 6.3. Radiative transfer equation

The RTE describes the radiative intensity field within an enclosure as a function of location, direction and spectral variables. The net radiative heat transfer over a surface is the sum of the contributions of radiative energy irradiating the surface from all possible directions and for all possible wavenumbers [98]. Thus, solving the RTE in a coupled heat transfer problem requires simplification in order to reduce the computation time required.

The RTE in a semi-transparent medium that absorbs, emits and scatters radiation as a function of the wavelength is [96]:

$$\frac{di_\lambda}{ds} = \underbrace{a_\lambda \cdot i_{\lambda b}(s)}_A - \underbrace{(a_\lambda + \sigma_\lambda) \cdot i_\lambda(s)}_B + \underbrace{\frac{\sigma_\lambda}{4\pi} \cdot \int_{4\pi} i_\lambda(s, \omega_i) \cdot \Phi_\lambda(\omega_i, \omega) \cdot d\omega_i}_C \quad (20)$$

Eq. (20) describes the intensity variation ( $i_\lambda$ ) of a photon travelling through a radiatively participating medium in direction  $s$ . The change is due to a gain in intensity by emission (A) and scattering (C) and the losses by absorption and scattering (B) [102].

With the spectral intensity  $i_\lambda$  given as the solution of the RTE, the divergence of the spectral radiative heat transfer can be calculated as follows [96]:

$$\nabla q_{r,\lambda} = a_\lambda \cdot (4 \cdot \pi \cdot i_{\lambda b} - G_\lambda) \quad (21)$$

In Eq. (21), the spectral blackbody intensity  $i_{\lambda b}$  is given by Planck's law and the spectral incident radiation  $G_\lambda$  is given by the following expression:

$$G_\lambda = \int_{4\pi} i_\lambda d\omega \quad (22)$$

The divergence of the total radiative heat transfer necessary to couple it with the solid energy equation is obtained by integration over the entire spectrum:

$$\nabla q_r = \int_0^\infty \nabla q_{r,\lambda} \cdot d\lambda \quad (23)$$

Several approximations have been adopted in the literature to reduce its complexity. In the following, the main approximations are presented.

#### 6.3.1. Rosseland approximation

The Rosseland approximation is a simple expression for radiative heat transfer. It is used for optically thick media, where the optical thickness is much greater than unity.

Despite the Rosseland approximation having low accuracy near boundaries as a result of the large temperature difference between both volumetric absorber phases, it is usually adopted due to its simplicity. The Rosseland approximation assumes radiation inside the medium behaves like thermal diffusion. Thus, it is only affected by close neighbours. The radiation problem is reduced to a simple conduction problem with conductivity strongly dependent on temperature. It is implemented by modifying the conduction term in the solid energy equation.

$$\nabla q_r = -\nabla \left( \frac{16\sigma_{SB}T_s^3}{3\beta} \nabla T_s \right) = -\nabla (k_r \nabla T_s) \quad (24)$$

The boundary condition for the Rosseland approximation takes into account the radiative losses from the volumetric frontal surface, without reflection and back-scattering, as radiation is total absorbed and then behaves as conduction:

$$(k_{eff,s} \nabla T_s) = I_0 - \varepsilon \sigma_{SB} (T_s^4 - T_{amb}^4) \quad (25)$$

Usually, convective losses from the porous inlet are negligible compared to thermal losses.



### 6.3.2. P<sub>1</sub> approximation

This radiative model comes from the spherical harmonics method, also known as the moment method. The great advantage of the spherical harmonics method is the conversion of the radiative transfer equation into a relatively simple partial differential equation. The drawback is that the lowest-order is only accurate with near-isotropic radiative intensity, and the accuracy improvement for the higher-order is reduced [98].

The P<sub>1</sub>-approximation is the lowest-order of the spherical harmonics series with two terms: The first is the total incident radiation:  $i^0 = G$ , and the second is the radiative heat transfer:  $i^1 = q_r$  [98]. This method can be used with different scattering phase functions; however, isotropic scattering is usually adopted [87, 90, 103]. The boundary condition leads to:

$$\nabla q_r = a \cdot (4 \cdot \pi \cdot i_b - G) \quad (26)$$

$$\frac{1}{(3 \cdot (a + \sigma) - c \cdot \sigma)} \cdot \nabla G = -q_r \quad (27)$$

Combining previous equations leads to a single diffusion equation for the total incident radiation, G:

$$-\nabla \cdot (\Gamma \cdot \nabla G) = a \cdot (4 \cdot \pi \cdot i_b - G) = a \cdot (4 \cdot \sigma_{SB} \cdot T_s^4 - G) \quad (28)$$

After solving for total incident radiation, G, the divergence of the radiative heat transfer is computed with Eq. (26), leading to the source term needed for the solid energy equation.

The Marshak boundary condition applies to the P<sub>1</sub> approximation, and it takes into account the thermal losses coming from the absorber after partial interception of the incident solar flux:

$$\frac{-1}{3 \cdot \beta} \cdot \nabla G = I_0 - \frac{G(0)}{2} \quad (29)$$

### 6.3.3. Discrete ordinate method

The discrete ordinate method transforms the radiative transfer equation into a set of partial differential equations. This method is based on a discrete representation of the directional variation of radiative intensity. Thus, the total solid angle is discretized, and the radiative transfer equation is solved along the optical path for each discretized solid angle [104]. The discrete ordinate method is suitable for working with high participative media and has good directional accuracy.

### 6.3.3.1. Two-flux approximation

The two-flux approximation is a specific case of the discrete ordinate method based on the discretization of the space into two hemispheres: forward (+) and backward (-). This method has low computational resource requirements, and isotropic scattering is usually accepted in both hemispheres [10], leading to the following two equations for the forward and backward intensities,  $i^+$  and  $i^-$  [98]:

$$\begin{aligned} \frac{1}{2\beta} \cdot \nabla i^+ &= -i^+ + \frac{\Omega}{2} \cdot (i^+ + i^-) + (1 - \Omega) \cdot \phi \cdot i_b \\ -\frac{1}{2\beta} \cdot \nabla i^- &= -i^- + \frac{\Omega}{2} \cdot (i^+ + i^-) + (1 - \Omega) \cdot \phi \cdot i_b \end{aligned} \quad (30)$$

When a pseudo-surface is used as a boundary condition [10], the emission term is multiplied by the porosity, to represent the fact that the internal emission in the bulk absorber propagates in the void space only, not in the entire volume [105].

Once Eq. (30) are solved the net radiative heat transfer is  $q_r = \pi \cdot (i^+ - i^-)$ , and the net radiative heat source per unit volume absorbed is given by the divergence of the radiative heat transfer (to be implemented in the solid energy equation):

$$-\nabla q_r = -a [4 \cdot \sigma_{SB} \cdot T_s^4 - 2\pi \cdot (i^+ + i^-)] \quad (31)$$

The two differential equations describing the forward and backward intensities,  $i^+$  and  $i^-$ , uses the following boundary conditions [70]:

$$\begin{aligned} i^+ &= \frac{I_0}{\pi} \\ i^- &= \frac{\sigma_{SB} T_s^4}{\pi} \end{aligned} \quad (32)$$

### 6.3.3.2. S<sub>4</sub> approximation

The discrete ordinate method is solved for a set of different directions and the integrals over direction are replaced by numerical quadratures. The choice of quadrature is arbitrary, although restrictions on the directions and quadrature weights may arise from the desire to preserve symmetry. The most commonly used Sn-approximations are S<sub>2</sub>, S<sub>4</sub>, S<sub>6</sub> and S<sub>8</sub> [98].

The second lower order formulation, S<sub>4</sub>, is presented with 24 ordinates, and is widely used in the literature [10, 76]. This formulation needs to solve four ordinates, two in the forward direction and two in the backward ( $i_j^+ - i_j^-$ , where  $j=1, 2$ ). The higher the formulation order, the better the representation of the directional incident radiation within participative media. The following two equations for the forward and backward intensities,  $i_j^+$  and  $i_j^-$ , are derived:

$$\begin{aligned} \frac{\mu_j}{\beta} \cdot \nabla i_j^+ &= (1 - \Omega) \cdot \phi \cdot i_b - i_j^+ + \frac{\Omega}{4\pi} \sum_{k=1}^{24} w_k \cdot (i_k^+ + i_k^-) \cdot \Phi_{jk} \\ -\frac{\mu_j}{\beta} \cdot \nabla i_j^- &= (1 - \Omega) \cdot \phi \cdot i_b - i_j^- + \frac{\Omega}{4\pi} \sum_{k=1}^{24} w_k \cdot (i_k^+ + i_k^-) \cdot \Phi_{jk} \end{aligned} \quad (33)$$

The same consideration for the emission term presented in the previous section applies in Eq. (33).

The radiative heat source to be implemented in the solid energy equation is:

$$-\nabla q_r = \sum_{j=1}^2 w_j' \cdot \mu_j \cdot (\nabla i_j^+ + \nabla i_j^-) \quad (34)$$

For the  $S_4$  approximation, the boundary conditions are highly dependent on the problem formulation. Kribus and co-workers [10] and Zaversky and co-workers [76] present two different boundary conditions for two different setups.

#### 6.3.4. Monte Carlo method

The Monte Carlo method refers to any strategy for solving a mathematical issue with an appropriate statistical technique. This method involves tracing the path of a significant number of photons from an emission point to an absorption point. The main characteristic is that the most complex problems can be solved relatively easily [98]. The main weakness is that a Monte Carlo simulation may be too computationally expensive to be practical with realistic geometric features.

Among more recent methodological advances, the zero-variance concept and the sensitivity estimation theoretical framework are the most commonly adopted techniques, as both can be at least partially translated into simple systematic procedures in the solar context. Both rely on a full explicitation of the strict relationship between a linear transport Monte Carlo algorithm and an integral transport formulation [106].

The Monte Carlo method solves the integral radiative equation to implement its solution as a source term in the solid energy equation.

It should be noted, that the Monte Carlo strategy should include the discretization of the incident and scattering directions. Usually, the photon travelling through the medium is generated arbitrarily by means of a probability density function which depends on the scattering coefficients. Moreover, the absorption has to be accounted for through the photon path.

The Monte Carlo approach is the most accurate for calculating the radiative heat flux inside a VA's porous medium. When coupled with a CFD model it also yields the most accurate results at the pore level.

The best modelling strategy is the following: the Monte Carlo technique is first used to determine the solar distribution inside an absorber, which is then passed to a CFD model to solve the governing microscopic equations. Such a procedure is extremely complicated and has very high computational demands. For example, Du and co-workers [62] solved all the governing equations with CFD software, updating the radiative heat flux every ten iterations to converge on a solution.

## 6.4. Summary

The methods available to solve the radiative heat transfer inside a VA have been presented. This section deals with concerns about linking each simulation technique with an appropriate method as shown in Fig. 7:

- 1) Detail simulation: This method is directly linked to the CFD model and 3D. The most suitable radiation approach for this technique is linked to the morphological structure of the absorber. Two classifications appear:
  - a) Periodical structure with relative simple geometry: The absorber rarely has a periodical structure with relative simple geometry. However, there are a few cases, like the pin-shaped geometry (Fig. 5c) or the single channel of a honeycomb (Fig. 5d). For such cases, the direct exchange area method is the preferred option due to its high accuracy and acceptable computing demand. Nevertheless, some authors [59] have considered the analytical simplified method despite it fails to capture the details of the radiative process inside the absorber.
  - b) Periodical or Non-Periodical structure with complex geometry: The absorber is normally a complex structure with a multitude of interlocking shapes, following a random pattern (Fig. 4c, Fig. 5a, Fig. 5e). These complex geometries account for the radiative heat transfer interaction with an absorbing, emitting, and scattering medium. Thus, the radiative transfer equation requires a solution that is normally the Monte Carlo approach.
- 2) Homogeneous equivalent model: This method considers the volume of the absorber as a porous continuum, thus the direct exchange area method is avoided by definition. Then, the solution of the radiative heat transfer is adopted from the remaining choices:
  - a) 1D: This technique, HEM+1D, is able to solve all the radiative transfer equation approximations available in the literature. So, the adopted method is a trade-off between accuracy and computational resources.
  - b) CFD: This technique presents limitations for solving any radiative transfer equation approximation (section 6.3) in a continuum model. The different approximations should be implemented by means of User Defined Functions [101]. This limitation avoids the implementation of the most accurate methods. Thus, most of the studies use the optically thick media approach (Rosseland and  $P_1$ -approximations). Nevertheless, there are complex strategies which use the more accurate discrete ordinate method [107], which carries with it a great deal of labour.

Fig. 7 shows the available choices for the radiative heat transfer once the simulation method and the model are selected. The final decision is a trade-off between complexity and computational resources.

Overall, the Monte Carlo technique is the most adequate approach for the computation of the radiation inside any type of absorber whatever the morphology, but if the time factor is a limitation, the direct exchange area method is the best choice for DS, and the discrete ordinate method is recommended due to its high accuracy for the HEM. Kribus and co-workers compared different radiation methods in [10].

However, whichever radiative heat transfer method is adopted, particular attention should be given to the boundary condition as their correct selection greatly influences the results.

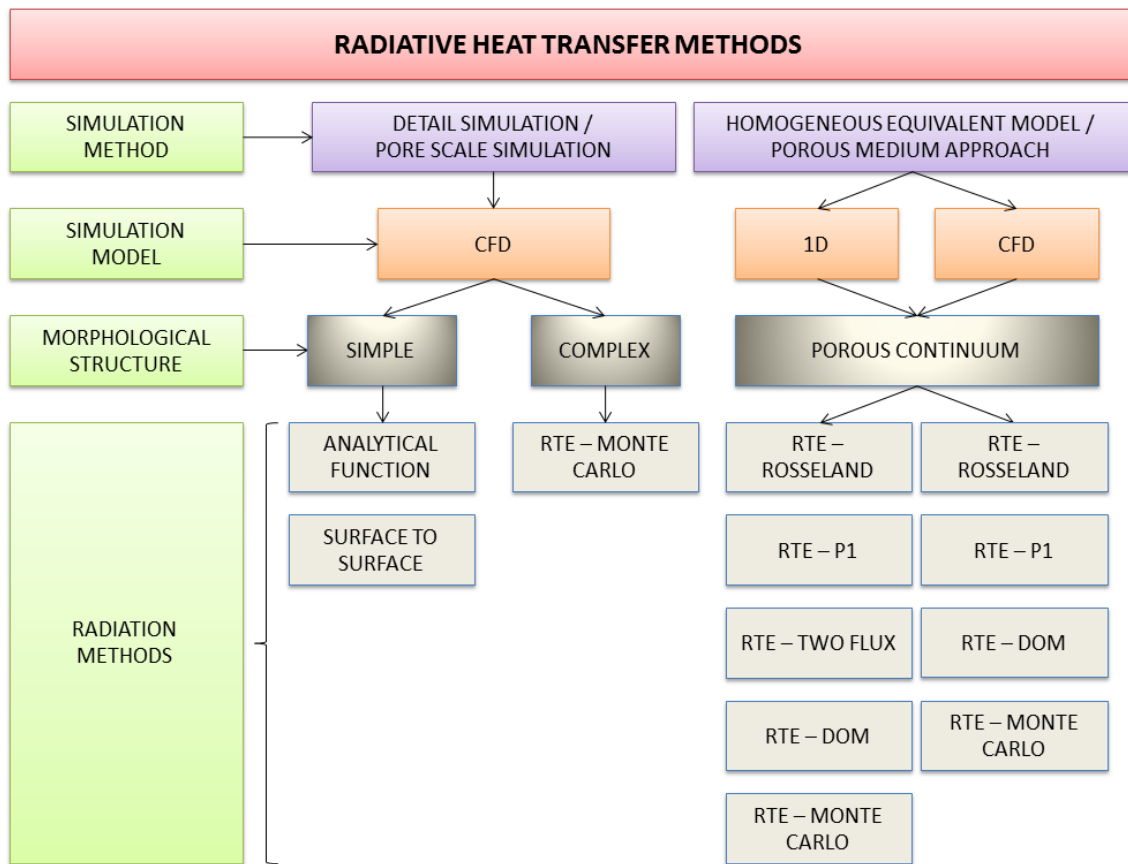


Fig. 7. Radiative heat transfer methods which apply to the analysis of volumetric absorber performance

## 7. Outlook and conclusions

CSP technology with volumetric absorbers (VA) using air is attracting a great deal of attention, as it presents important environmental and technical advantages despite its delayed commercial implementation resulting from some significant challenges, such as the theoretical volumetric effect that not having been shown to produce a significant advantage in the few experimental works that have achieved it.

In order to answer some open questions regarding VA technology, and to find new morphological configurations with high thermal and optical performance, an adequate modelling strategy is crucial to correctly predicting it. In that sense, this work has presented the main simulation strategies for the VA, together with a comprehensive literature review of the most important and most recent works.

The two main methodologies, detail simulation (DS) and the homogeneous equivalent method (HEM), the main models, CFD and 1D, and the equilibrium states, LTE and LTNE, have been described together with the main research literature. Concerning the radiative heat transfer inside the absorber, the main approaches available are described: 1) Beer's law, 2) Direct exchange surface area method, together with 3) four approaches to solving the radiative transfer equation in participative medium: a) Rosseland approximation, b)  $P_1$  approximation, c) Discrete ordinate method, and d) Monte Carlo method.

DS solves microscopic equations without adding empirical terms producing the most accurate approach, but it presents some limitations: the porous geometry is extremely complicated in most cases, and the computational resources needed become prohibitively high. Thus, there are few works in the literature about the overall analysis of VA performance. This paper presents thirteen studies using detail simulation strategies. Among them, eight are simplified DSs (sDSs), which focus on the numerical determination of effective properties, while five deal with the complete simulation (DS) of the absorber. The former studies did not need to solve for the radiation inside the absorber, while later work used different approaches. Usually, relatively simple geometries used the direct exchange surface area method because it is simpler and has good accuracy; however, there are highly participative absorbers, such as unstructured foams, where the Monte Carlo approach is the best and most accurate choice.

HEM is a less time-consuming method and simplifies the real geometry of a porous continuum, but its accuracy is related to the quality of the effective properties adopted in the macroscopic equations and the radiative method applied. This study presents twenty-nine works using the homogeneous equivalent method, eleven adopting a 1D model, mainly focused on parametric and optimisation analysis, study of fluid instabilities, and analysis of different radiative models, and eighteen works adopting a CFD model, where several effects were analysed, such as composite or graded absorbers, Gaussian incident profiles, windowed receivers, etc. Among them, twenty-six considered unstructured foams as the preferred geometry, twenty-four works used the LTNE approach, and twenty-two adopted the optically thick approach (Rosseland and  $P_1$  approximations) for the radiative heat transfer. Concerning morphological configuration, the research is focused on the optimisation of foams as they seem to offer the best performing configuration; concerning equilibrium state, the LTNE is highly recommended as it gives more information than the unrealistic LTE approach which is inadequate for a real analysis of the absorber; and finally concerning radiative heat transfer, the optically thick approach is mostly adopted since it is quite easy and fast, but its accuracy is pretty limited especially near the boundaries. So, as mentioned before, for highly participative medium, i.e. foams, the Monte Carlo approach is the preferable choice, and the second possible choice is the discrete ordinate method which has been shown to perform quite reliably when compared to the Monte Carlo approach.

Of the thirteen and twenty-nine DS and HEM studies, respectively, presented here, seven DS and twenty HEM studies have been published within the last five years. Obviously, not all the VA modelling studies have been presented in this review, but the most important and representative ones have. However, the fact that nearly 65% of the studies have been published in the last five years provides a measure of the increasing interest in VAs.

This review presents the following conclusions:

1. It is assumed that the feasibility of the air technology lies in the volumetric effect, otherwise, the receiver thermal efficiency is limited due to the higher thermal losses. This theoretical effect is difficult to achieve in real conditions, and when it has been demonstrated experimentally (just in two works [11, 13]), the improvement in the thermal performance has not been assured.
2. There are several assumptions that should be avoided when volumetric absorber performance is analysed: a) the LTE approach which produces the volumetric effect by definition, could lead to the erroneous assumption that the volumetric absorber would almost automatically have a volumetric effect, b) Beer's law is a quite limited approach for the analysis of radiative heat transfer inside a

porous absorber and should be omitted or used only as a preliminary analysis.

3. The most widely used numerical methodology for the evaluation of the absorber's fluid and thermal performance is the HEM using the CFD model together with the LTNE approach, and the optically thick approach which is an acceptable initial approximation at the engineering level.
4. The most accurate strategy for the simulation of a porous absorber is the DS using the discrete ordinate method or the Monte Carlo methods for the computation of the radiative heat transfer as both options are the most accurate for predicting the real performance of the absorber under real working conditions. This modelling strategy offers the opportunity to answer important open questions, and give the chance to check if air technology could be implemented commercially.
5. The correct selection of the boundary conditions for both simulation strategies, and especially for the radiative heat transfer mechanism, is crucial to assess reliable final results.

## **Acknowledgment**

The author wish to thank “Comunidad de Madrid” and “European Social Fund” for its financial support to the ALCCONES project through the Programme of Activities between Research Groups (S2013/MAE-2985), to the “DETECSOL” project funded by the Spanish government with ERDF funds with reference ENE2014-56079-R, and to the “SOLTERMIN” project funded by the Spanish government with ERDF funds with reference ENE2017-83973-R.



## References

- [1] Sizmann RL. Solar radiation conversion. Solar power plants. Fundamentals, technology, systems, economics. 1st ed. Berlin: Springer Verlag; 1991.
- [2] Ho CK. Advances in central receivers for concentrating solar applications. *Sol Energy*. 2017;152:38-56.
- [3] Zhang HL, Baeyens J, Degève J, Cacères G. Concentrated solar power plants: Review and design methodology. *Renew Sustain Energy Rev*. 2013;22:466-81.
- [4] Islam MT, Huda N, Abdullah AB, Saidur R. A comprehensive review of state-of-the-art concentrating solar power (CSP) technologies: Current status and research trends. *Renew Sustain Energy Rev*. 2018;91:987-1018.
- [5] Avila-Marin AL, Fernandez-Reche J, Tellez FM. Evaluation of the potential of central receiver solar power plants: Configuration, optimization and trends. *Appl Energy*. 2013;112:274-88.
- [6] Behar O, Khellaf A, Mohammedi K. A review of studies on central receiver solar thermal power plants. *Renew Sustain Energy Rev*. 2013;23:12-39.
- [7] Romero M, Buck R, Pacheco JE. An update on solar central receiver systems, projects, and technologies. *J Sol Energy Eng*. 2002;124:98-108.
- [8] Avila-Marin AL. Volumetric receivers in solar thermal power plants with central receiver system technology: A review. *Sol Energy*. 2011;85:891-910.
- [9] Fricker HW. Proposal for a novel type of solar gas receiver. In: *Proceedings of the International Seminar on Solar Thermal Heat Production*. Stuttgart, Germany. 1983.
- [10] Kribus A, Gray Y, Grijnevich M, Mittelman G, Mey-Cloutier S, Caliot C. The promise and challenge of solar volumetric absorbers. *Sol Energy*. 2014;110:463-81.
- [11] Menigault T, Flamant G, Rivoire B. Advanced high-temperature two-slab selective volumetric receiver. *Sol Energy Mater*. 1991;24:192-203.
- [12] Alberti F, Santiago S, Roccabruna M, Luque S, Gonzalez-Aguilar J, Crema L, et al. Numerical analysis of radiation propagation in innovative volumetric receivers based on selective laser melting techniques. *AIP Conf Proc*. 2016;1734:030001.
- [13] Luque S, Menéndez G, Roccabruna M, González-Aguilar J, Crema L, Romero M. Exploiting volumetric effects in novel additively manufactured open solar receivers. *Sol Energy*. 2018;174:342-51.
- [14] Hoffschmidt B. Vergleichende bewertung verschiedener konzepte volumetrischer strahlungsempfänger. Cologne, Germany: DLR - Forschungsberichte; 1997.
- [15] Capuano R, Fend T, Schwarzbözl P, Smirnova O, Stadler H, Hoffschmidt B, et al. Numerical models of advanced ceramic absorbers for volumetric solar receivers. *Renew Sustain Energy Rev*. 2016;58:656-65.
- [16] Mey-Cloutier S, Caliot C, Kribus A, Gray Y, Flamant G. Experimental study of ceramic foams used as high temperature volumetric solar absorber. *Sol Energy*. 2016;136:226-35.
- [17] Gomez-Garcia F, González-Aguilar J, Olalde G, Romero M. Thermal and hydrodynamic behavior of ceramic volumetric absorbers for central receiver solar power plants: A review. *Renew Sustain Energy Rev*. 2016;57:648-58.
- [18] Avila-Marin AL, Alvarez de Lara M, Fernandez-Reche J. Experimental results of gradual porosity volumetric air receivers with wire meshes. *Renew Energy*. 2018;122:339-53.
- [19] Pabst C, Feckler G, Schmitz S, Smirnova O, Capuano R, Hirth P, et al. Experimental performance of an advanced metal volumetric air receiver for solar towers. *Renew Energy*. 2017;106:91-8.
- [20] Avila-Marin AL, Alvarez-Lara M, Fernandez-Reche J. Experimental results of gradual porosity wire mesh absorber for volumetric receivers. *Energy Procedia*. 2014;49:275-83.
- [21] Livshits M, Avivi L, Kribus A. Dense wire mesh as a high-efficiency solar volumetric absorber. In: *Proceedings of the ASME Summer Heat Transfer Conference*. Bellevue, Washington, USA. 2017.
- [22] Roldán MI, Avila-Marin A, Alvarez-Lara M, Fernandez-Reche J. Experimental and numerical characterization of ceramic and metallic absorbers under lab-scale conditions. *Energy Procedia*. 2015;69:523-31.
- [23] Meinecke W, Cordes S. Phoebus technology program solar air receiver (TSA)-Operational experience and test evaluation of the 2.5 MWth volumetric air receiver test facility at the Plataforma Solar de Almeria. In: *Proceedings of the 7th SolarPACES Conference*. Moscow, Russia. 1994.
- [24] Meinecke W, Cordes S, Merten I. Phoebus technology program solar air receiver (TSA) - Final report on test evaluation. Cologne, Germany: DLR; 1994.
- [25] Haeger M, Keller L, Monterreal R, Valverde A. Phoebus technology program solar air receiver (TSA): Experimental set up for TSA at the CESA test facility of the Plataforma Solar de Almeria (PSA). In: *Proceedings of the ISES Conference*. San Francisco, California, USA. 1994.

- [26] Téllez F, Romero M, Heller P, Valverde A, Fernandez-Reche J, Ulmer S, et al. Thermal performance of “SolAir 3000 kWth” ceramic volumetric solar receiver. In: Proceedings of the 12th SolarPACES. Oaxaca, Mexico. 2004.
- [27] Tescari S, Singh A, Agrafiotis C, de Oliveira L, Breuer S, Schlögl-Knothe B, et al. Experimental evaluation of a pilot-scale thermochemical storage system for a concentrated solar power plant. *Appl Energy*. 2017;189:66-75.
- [28] Kronhardt V, Alexopoulos S, Reißel M, Latzke M, Rendón C, Sattler J, et al. Simulation of operational management for the solar thermal test and demonstration power plant jülich using optimized control strategies of the storage system. *Energy Procedia*. 2015;69:907-12.
- [29] Koll G, Schwarzbozl P, Hennecke K, Hartz T, Schmitz M, Hoffschmidt B. The solar tower Jülich – A research and demonstration plant for central receiver systems. In: Proceedings of the 15th SolarPACES conference. Berlin, Germany. 2009.
- [30] Hennecke K, Schwarzbozl P, Alexopoulos S, Hoffschmidt B, Götsche J, Koll G, et al. Solar power tower Jülich – The first test and demonstration plant for open volumetric receiver technology in Germany. In: Proceedings of the 14th SolarPACES conference. Las Vegas, USA. 2008.
- [31] Heller P, Pfänder M, Denk T, Tellez F, Valverde A, Fernandez J, et al. Test and evaluation of a solar powered gas turbine system. *Sol Energy*. 2006;80:1225-30.
- [32] CENER. CAPTure - Competitive SolAr Power Towers, Grant Agreement Number 640905. [www.capture-solar-energy.eu/2015](http://www.capture-solar-energy.eu/2015).
- [33] Zaversky F, Aldaz L, Sánchez M, Fernandez-Reche J, Füßel A, Adler J. Experimental and numerical evaluation of a small array of ceramic foam volumetric absorbers. In: Proceedings of the 24th SolarPACES. Casablanca, Morocco 2018.
- [34] Zaversky F, Sánchez M, Roldán MI, Ávila-Marín AL, Füßel A, Adler J, et al. Experimental evaluation of volumetric solar absorbers – Ceramic foam vs. an innovative rotary disc absorber concept. *AIP Conf Proc*. 2018;2033:040044.
- [35] Barreto G, Canhoto P, Collares-Pereira M. Three-dimensional modelling and analysis of solar radiation absorption in porous volumetric receivers. *Appl Energy*. 2018;215:602-14.
- [36] Mahdi RA, Mohammed HA, Munisamy KM, Saeid NH. Review of convection heat transfer and fluid flow in porous media with nanofluid. *Renew Sustain Energy Rev*. 2015;41:715-34.
- [37] Chavez JM, Chaza C. Testing of a porous ceramic absorber for a volumetric air receiver. *Sol Energy Mater*. 1991;24:172-81.
- [38] Pitot de la Beaujardiere J-FP, Reuter HCR. A review of performance modelling studies associated with open volumetric receiver CSP plant technology. *Renew Sustain Energy Rev*. 2018;82:3848-62.
- [39] Avila-Marin AL, Alvarez-Lara M, Fernandez-Reche J. A regenerative heat storage system for central receiver technology working with atmospheric air. *Energy Procedia*. 2014;49:705-14.
- [40] Zanganeh G, Pedretti A, Zavattoni S, Barbato M, Steinfeld A. Packed-bed thermal storage for concentrated solar power – Pilot-scale demonstration and industrial-scale design. *Sol Energy*. 2012;86:3084-98.
- [41] Pacio J, Singer C, Wetzel T, Uhlig R. Thermodynamic evaluation of liquid metals as heat transfer fluids in concentrated solar power plants. *Appl Therm Eng*. 2013;60:295-302.
- [42] Pitot de la Beaujardiere J-FP, Reuter HCR, Klein SA, Reindl DT. Impact of HRSG characteristics on open volumetric receiver CSP plant performance. *Sol Energy*. 2016;127:159-74.
- [43] Becker M, Fend T, Hoffschmidt B, Pitz-Paal R, Reutter O, Stamatov V, et al. Theoretical and numerical investigation of flow stability in porous materials applied as volumetric solar receivers. *Sol Energy*. 2006;80:1241-8.
- [44] Kribus A, Ries H, Spirkel W. Inherent limitations of volumetric solar receivers. *J Sol Energy Eng*. 1996;118:151-5.
- [45] Vafai K. Handbook of porous media. 3rd ed. Boca Raton: Taylor & Francis; 2015.
- [46] Vafai K, Tien CL. Boundary and inertia effects on flow and heat transfer in porous media. *Int J Heat Mass Transf*. 1981;24:195-203.
- [47] Wang P, Vafai K, Liu DY. Analysis of the volumetric phenomenon in porous beds subject to irradiation. *Numer Heat Transf A-Appl*. 2016;70:567-80.
- [48] Spirkel W, Ries H, Kribus A. Performance of surface and volumetric solar thermal absorbers. *J Sol Energy Eng*. 1997;119:152-5.
- [49] Zhao CY, Tassou SA, Lu TJ. Analytical considerations of thermal radiation in cellular metal foams with open cells. *Int J Heat Mass Transf*. 2008;51:929-40.
- [50] Petrasch J, Meier F, Friess H, Steinfeld A. Tomography based determination of permeability, Dupuit–Forchheimer coefficient, and interfacial heat transfer coefficient in reticulate porous ceramics. *Int J Heat Fluid Flow*. 2008;29:315-26.

- [51] Petrasch J, Wyss P, Steinfeld A. Tomography-based Monte Carlo determination of radiative properties of reticulate porous ceramics. *J Quant Spectrosc Ra*. 2007;105:180-97.
- [52] Wu Z, Caliot C, Bai F, Flamant G, Wang Z, Zhang J, et al. Experimental and numerical studies of the pressure drop in ceramic foams for volumetric solar receiver applications. *Appl Energy*. 2010;87:504-13.
- [53] Wu Z, Caliot C, Flamant G, Wang Z. Numerical simulation of convective heat transfer between air flow and ceramic foams to optimise volumetric solar air receiver performances. *Int J Heat Mass Transf*. 2011;54:1527-37.
- [54] Zafari M, Panjepour M, Davazdah Emami M, Meratian M. Microtomography-based numerical simulation of fluid flow and heat transfer in open cell metal foams. *Appl Therm Eng*. 2015;80:347-54.
- [55] Zhao Y, Tang GH. Monte Carlo study on extinction coefficient of silicon carbide porous media used for solar receiver. *Int J Heat Mass Transf*. 2016;92:1061-5.
- [56] Avila-Marin AL, Fernandez-Reche J, Casanova M, Caliot C, Flamant G. Numerical simulation of convective heat transfer for inline and stagger stacked plain-weave wire mesh screens and comparison with a local thermal non-equilibrium model. *AIP Conf Proc*. 2017;1850:030003.
- [57] Avila-Marin AL, Caliot C, Flamant G, Alvarez de Lara M, Fernandez-Reche J. Numerical determination of the heat transfer coefficient for volumetric air receivers with wire meshes. *Sol Energy*. 2018;162:317-29.
- [58] Michailidis N, Stergioudi F, Omar H, Missirlis D, Vlahostergios Z, Tsipas S, et al. Flow, thermal and structural application of Ni-foam as volumetric solar receiver. *Sol Energy Mater Sol Cells*. 2013;109:185-91.
- [59] Fend T, Schwarzbözl P, Smirnova O, Schöllgen D, Jakob C. Numerical investigation of flow and heat transfer in a volumetric solar receiver. *Renew Energy*. 2013;60:655-61.
- [60] Capuano R, Fend T, Stadler H, Hoffschmidt B, Pitz-Paal R. Optimized volumetric solar receiver: Thermal performance prediction and experimental validation. *Renew Energy*. 2017;114:556-66.
- [61] Cagnoli M, Savoldi L, Zanino R, Zaversky F. Coupled optical and CFD parametric analysis of an open volumetric air receiver of honeycomb type for central tower CSP plants. *Sol Energy*. 2017;155:523-36.
- [62] Du S, Li M-J, Ren Q, Liang Q, He Y-L. Pore-scale numerical simulation of fully coupled heat transfer process in porous volumetric solar receiver. *Energy*. 2017;140:1267-75.
- [63] Hinze JO. *Turbulence*. 2nd ed. New York: McGraw Hill; 1975.
- [64] Sadouk HC. *Modelisation de l'encrassement en regime turbulent dans un echangeur de chaleur a plaques avec un revetement breux sur les parois* [doctoral thesis]. Paris, France: Universite Paris-Est; 2009.
- [65] Vafai K. *Handbook of porous media*. 2nd ed. Boca Raton: Taylor & Francis; 2005.
- [66] Pitz-Paal R, Hoffschmidt B, Böhmer M, Becker M. Experimental and numerical evaluation of the performance and flow stability of different types of open volumetric absorbers under non-homogeneous irradiation. *Sol Energy*. 1997;60:135-50.
- [67] Bai F. One dimensional thermal analysis of silicon carbide ceramic foam used for solar air receiver. *Int J Therm Sci*. 2010;49:2400-4.
- [68] Xu C, Song Z, Chen L-d, Zhen Y. Numerical investigation on porous media heat transfer in a solar tower receiver. *Renew Energy*. 2011;36:1138-44.
- [69] Sano Y, Iwase S, Nakayama A. A local thermal nonequilibrium analysis of silicon carbide ceramic foam as a solar volumetric receiver. *J Sol Energy Eng*. 2012;134:021006--8.
- [70] Mey S, Caliot C, Flamant G, Kribus A, Gray Y. Optimization of high temperature SiC volumetric solar absorber. *Energy Procedia*. 2014;49:478-87.
- [71] Wang P, Vafai K, Liu DY. Analysis of radiative effect under local thermal non-equilibrium conditions in porous media-Application to a solar air receiver. *Numer Heat Transf A-Appl*. 2014;65:931-48.
- [72] Li Q, Bai F, Yang B, Wang Z, El Hefni B, Liu S, et al. Dynamic simulation and experimental validation of an open air receiver and a thermal energy storage system for solar thermal power plant. *Appl Energy*. 2016;178:281-93.
- [73] Wang P, Vafai K. Modeling and analysis of an efficient porous media for a solar porous absorber with a variable pore structure. *J Sol Energy Eng*. 2017;139:051005--7.
- [74] Wang P, Li JB, Bai FW, Liu DY, Xu C, Zhao L, et al. Experimental and theoretical evaluation on the thermal performance of a windowed volumetric solar receiver. *Energy*. 2017;119:652-61.
- [75] Karr K, Dybbs A. Internal heat transfer coefficients of porous metals. In: *Proceedings of the ASME Winter Annual Meeting*. Phoenix, Arizona. 1982.

- [76] Zaversky F, Aldaz L, Sánchez M, Ávila-Marín AL, Roldán MI, Fernández-Reche J, et al. Numerical and experimental evaluation and optimization of ceramic foam as solar absorber – Single-layer vs multi-layer configurations. *Appl Energy*. 2018;210:351-75.
- [77] Wu Z, Caliot C, Flamant G, Wang Z. Coupled radiation and flow modeling in ceramic foam volumetric solar air receivers. *Sol Energy*. 2011;85:2374-85.
- [78] Wu Z, Wang Z. Fully coupled transient modeling of ceramic foam volumetric solar air receiver. *Sol Energy*. 2013;89:122-33.
- [79] Cheng ZD, He YL, Cui FQ. Numerical investigations on coupled heat transfer and synthetical performance of a pressurized volumetric receiver with MCRT–FVM method. *Appl Therm Eng*. 2013;50:1044-54.
- [80] Wang F, Shuai Y, Tan H, Yu C. Thermal performance analysis of porous media receiver with concentrated solar irradiation. *Int J Heat Mass Transf*. 2013;62:247-54.
- [81] Wang F, Shuai Y, Tan H, Zhang X, Mao Q. Heat transfer analyses of porous media receiver with multi-dish collector by coupling MCRT and FVM method. *Sol Energy*. 2013;93:158-68.
- [82] Wang F, Tan J, Yong S, Tan H, Chu S. Thermal performance analyses of porous media solar receiver with different irradiative transfer models. *Int J Heat Mass Transf*. 2014;78:7-16.
- [83] Fuqiang W, Jianyu T, Lanxin M, Yong S, Heping T, Yu L. Thermal performance analysis of porous medium solar receiver with quartz window to minimize heat flux gradient. *Sol Energy*. 2014;108:348-59.
- [84] Roldán MI, Smirnova O, Fend T, Casas JL, Zarza E. Thermal analysis and design of a volumetric solar absorber depending on the porosity. *Renew Energy*. 2014;62:116-28.
- [85] Chen X, Xia X-L, Meng X-L, Dong X-H. Thermal performance analysis on a volumetric solar receiver with double-layer ceramic foam. *Energy Convers Manag*. 2015;97:282-9.
- [86] Meng X-l, Xia X-l, Zhang S-d, Sellami N, Mallick T. Coupled heat transfer performance of a high temperature cup shaped porous absorber. *Energy Convers Manag*. 2016;110:327-37.
- [87] Chen X, Xia X-L, Liu H, Li Y, Liu B. Heat transfer analysis of a volumetric solar receiver by coupling the solar radiation transport and internal heat transfer. *Energy Convers Manag*. 2016;114:20-7.
- [88] Roldán MI, Fernández-Reche J, Ballestrín J. Computational fluid dynamics evaluation of the operating conditions for a volumetric receiver installed in a solar tower. *Energy*. 2016;94:844-56.
- [89] Hoffschmidt B, Téllez FIM, Valverde A, Fernández Js, Fernández V. Performance evaluation of the 200-kWth HiTRec-II open volumetric air receiver. *J Sol Energy Eng*. 2003;125:87-94.
- [90] Chen X, Xia X-L, Yan X-W, Sun C. Heat transfer analysis of a volumetric solar receiver with composite porous structure. *Energy Convers Manag*. 2017;136:262-9.
- [91] Zhu Q, Xuan Y. Performance analysis of a volumetric receiver composed of packed shaped particles with spectrally dependent emissivity. *Int J Heat Mass Transf*. 2018;122:421-31.
- [92] Du S, He Y-L, Yang W-W, Liu Z-B. Optimization method for the porous volumetric solar receiver coupling genetic algorithm and heat transfer analysis. *Int J Heat Mass Transf*. 2018;122:383-90.
- [93] Teng L, Xuan Y. Thermal and hydrodynamic performance of a novel volumetric solar receiver. *Sol Energy*. 2018;163:177-88.
- [94] Du B-C, Qiu Y, He Y-L, Xue X-D. Study on heat transfer and stress characteristics of the pressurized volumetric receiver in solar power tower system. *Appl Therm Eng*. 2018;133:341-50.
- [95] Nimvari ME, Jouybari NF, Esmaili Q. A new approach to mitigate intense temperature gradients in ceramic foam solar receivers. *Renew Energy*. 2018;122:206-15.
- [96] Siegel R, Howell JR. Thermal radiation heat transfer. 4th ed. Great Britain: Taylor & Francis; 2002.
- [97] Avila-Marin AL, Caliot C, Alvarez de Lara M, Fernandez-Reche J, Montes MJ, Martinez-Tarifa A. Homogeneous equivalent model coupled with P1-approximation for dense wire meshes volumetric air receivers. *Renew Energy*. 2019;135:908-19.
- [98] Modest MF. Radiative heat transfer. 2nd ed. New York: McGraw Hill; 2003.
- [99] Gomez-Garcia F, Gonzalez-Aguilar J, Tamayo-Pacheco S, Olalde G, Romero M. Numerical analysis of radiation propagation in a multi-layer volumetric solar absorber composed of a stack of square grids. *Sol Energy*. 2015;121:94-102.
- [100] Perry RH, Green DW, Maloney JO. Perry's chemical engineers handbook. 7th ed. United States of America: McGraw Hill; 1999.
- [101] ANSYS-Fluent. Ansys Theory Guide. 2013.
- [102] Goebel F, Mundt C. Implementation of the P1 radiation model in the CFD solver NSMB and investigation of radiative heat transfer in the SSME main combustion chamber. In: Proceedings of the 17th AIAA International Space Planes and Hypersonic Systems and Technologies Conference. San Francisco, California, USA. 2011.
- [103] Wang P, Vafai K, Liu DY, Xu C. Analysis of collimated irradiation under local thermal non-equilibrium condition in a packed bed. *Int J Heat Mass Transf*. 2015;80:789-801.

- [104] Kumar S, Majumdar A, Tien CL. The differential-discrete-ordinate method for solutions of the equation of radiative transfer. *J Heat Transf.* 1990;112:424-9.
- [105] Taine J, Bellet F, Leroy V, Iacona E. Generalized radiative transfer equation for porous medium upscaling: Application to the radiative Fourier law. *Int J Heat Mass Transf.* 2010;53:4071-81.
- [106] Delatorre J, Baud G, Bézian JJ, Blanco S, Caliot C, Cornet JF, et al. Monte Carlo advances and concentrated solar applications. *Sol Energy.* 2014;103:653-81.
- [107] Gómez MA, Patiño D, Comesaña R, Porteiro J, Álvarez Feijoo MA, Míguez JL. CFD simulation of a solar radiation absorber. *Int J Heat Mass Transf.* 2013;57:231-40.